

**Synthesis and characterization of long afterglow phosphors
($\text{SrAl}_2\text{O}_4:\text{Ce}^{3+}$, $\text{SrAl}_2\text{O}_4:\text{Tb}^{3+}$, $\text{CaAl}_x\text{O}_y:\text{Tb}^{3+}$, $\text{Y}_3\text{Al}_5\text{O}_{12}:\text{Eu}^{3+}$) using
solution combustion method**

By

Foka Kewele Emily

A dissertation presented in fulfillment of the requirements for the degree

MAGISTER SCIENTIAE

Department of Physics

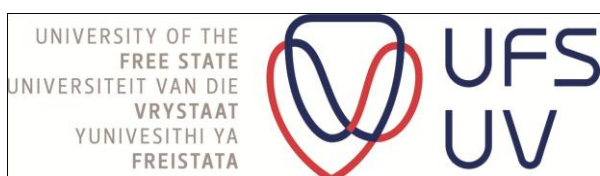
Faculty of Natural and Agricultural Science

University of the Free State

RSA

Supervisor: Prof. B F Dejene

Co-Supervisor: Prof H C Swart



November 2011

Dedicated to the memory of my late father

Tukele William Foka

Acknowledgements

My special thanks to:

- God Almighty for His grace, without Him this study wouldn't have been possible.
- My supervisor Prof. FB Dejene for his guidance, patience and valuable comments which were indispensable for the completion of my degree.
- My co-supervisor Prof. HC Swart for his valuable knowledge, helpful suggestions, and support.
- To all staff members of the Department of Physics UFS (Qwa Qwa Campus),
- My fellow researchers (Mantwa Lephoto, Amelia Tshabalala, Mduduze Mbongo, Halake Ali, Pontsho Mbule) and former UFS research student Dr. DB Bem for their assistance.
- Mart-Mari for her assistance and Mr. Hassan for helping with PL.
- South African National Research Foundation (NRF) and the University of the Free State for financial support.
- My family (brothers and sisters), my mother (Mapontsho Foka) for their love and moral support.
- My lovely son (Sibusiso), who has been a pride and joy to me. All the things that I have been doing all along in this study I was doing them for you.
- Last but not least, my love Lawrence for always been there for me.

Abstract

This work consists of several aspects of phosphor materials. Strontium, calcium and yttrium aluminate doped with rare earth (Ce, Tb and Eu) have been synthesized by solution combustion method using urea as a fuel for investigations of the luminescent, structure and morphological properties. The phosphors were characterized by several techniques such as X-ray diffraction (XRD), energy dispersive electroscopy (EDS), scanning electron microscopy (SEM), Fourier transform infrared spectroscopy (FTIR) and Photoluminescence (PL), PL data were collected using a Cary Eclipse Photoluminescence Spectrophotometer equipped with a 150 W xenon lamp.

Cerium doped strontium aluminum oxide ($\text{SrAl}_2\text{O}_4:\text{Ce}^{3+}$) were synthesized. The effects of different concentration of cerium were investigated. X-ray diffraction results confirmed the formation of the SrAl_2O_4 monoclinic phase (Powder Diffraction Standards (JCPDS) file No. 34-0379). The particle sizes of different peaks were estimated and the average particle size was 47 nm. SEM results showed agglomerated as well as small elongated-egg-like shape on particles when taken to higher magnification. The PL spectra show a broad emission consisting of two bands peaking at 374 and 384 nm, corresponding to the transitions from the lowest 5d excited state to the $^2\text{F}_{5/2}$ and $^2\text{F}_{7/2}$ states. The excitation and emission peak position shifted with varying the cerium concentration. This maybe due to uncontrollable electrospinning conditions like air and wetness, which influence the crystal field that surround Ce^{3+} .

$\text{SrAl}_2\text{O}_4:\text{Tb}^{3+}$ XRD peaks confirmed the formation of the SrAl_2O_4 monoclinic phase and some impurities were also observed. The photoluminescence characteristics show the emission peaks at 415, 436 and 459 nm which correspond to the $^5\text{D}_3$ to $^7\text{F}_j$ ($J=5, 4, \text{ and } 3$) level and 489, 543, 585, and 622 nm corresponding to $^5\text{D}_4$ to $^7\text{F}_j$ ($J= 6, 5, 4, 3$) under excitation at 229 nm and the terbium concentration was varied. The elements of the phosphor $\text{SrAl}_2\text{O}_4:\text{Tb}^{3+}$ were shown by energy dispersive spectroscopy. The decay curves were also observed and the decay constants show a higher value at a concentration of 0.25 mol% and lower value at a concentration of 2 mol%.

$\text{CaAl}_x\text{O}_y:\text{Tb}^{3+}$ green phosphors were obtained at low temperature (500 °C) by a solution-combustion method. The structural analysis revealed the presence of both monoclinic CaAl_4O_7 and CaAl_2O_4 . The main parent structure of CaAl_2O_4 monoclinic was revealed when

varying the concentration of terbium. The characteristic luminescence properties were investigated using emission spectra. The emission peaks are from transition of the 5D_4 state to the 7F_J ($J = 6, 5, 4, 3$) state. The optimal intensity was obtained when the concentration of Tb^{3+} was increased to 2 mol%. FTIR was used to identify all the chemical bands. Absorption bands of the condensed matter AlO_4 located in the range of 700 cm^{-1} - 900 cm^{-1} and condensed matter AlO_6 at 500 cm^{-1} - 680 cm^{-1} are attributed to AlO_4 liberation at 600 cm^{-1} - 900 cm^{-1} . The decay curves of the phosphor were investigated and showed a higher intensity and longer afterglow time at higher concentration of terbium 2 mol%. $Y_3Al_5O_{12}$ known as Yttrium aluminum garnet (YAG) phosphor doped with different concentration of Eu was synthesized by the solution combustion method. The crystalline structure, morphology and luminescent properties of the phosphors were studied. The SEM revealed the agglomerated morphology containing small spherical particles around the pores. FTIR spectra reveal all bonds that exist in the phosphor. The emission spectra revealed three major emission peaks at 592, 615, and 628 nm, corresponding to the $^5D_0 \rightarrow ^7F_1$ (592 nm), $^5D_0 \rightarrow ^7F_2$ (615 nm) and $^5D_0 \rightarrow ^7F_3$ (628 nm) transitions respectively. The luminescence intensity increased with an increase in Eu concentration at 0.7 mol% and then decreases with an increasing of concentration further.

Key words: rare earths, solution combustion process, long afterglow, luminescence

Acronyms

XRD—X-ray Diffraction

PL—Photoluminescence

EDS—Energy Dispersive Spectroscopy

SEM—Scanning Electron Microscopy

FTIR—Fourier Transform Infrared

Table of Contents

Abstract	iv
Chapter I: General introduction	1
1.1 Phosphor terminology and definition of phosphor.....	1
1.2 Long persistent phosphors (LPP).....	2
1.2.1 Methods to design Long Persistent Phosphor (LPP)	3
1.2.1.1 Co-doping	3
1.2.1.2 Persistent energy transfer.....	4
1.2.1.3 Doubly doped materials	4
1.3 Applications of phosphors	5
1.3.1 Fluorescent lamp.....	5
1.3.2 Cathode ray tube (CRT)	6
1.3.3 Flat panel display (FPD)	7
1.3.4 Other applications	8
1.3.4.1 Luminescent paints.....	8
1.3.4.1.1 Fluorescent paint	8
1.3.4.1.2 Phosphorescent paint	9
1.4 Fundamental of luminescence.....	10
1.4.1 Photoluminescence	10
1.4.2 Cathodoluminescence	11
1.4.3 Electroluminescence	12
1.4.4 Chemiluminescence	13
1.4.5 Bioluminescence.....	14
1.5 Statement of problem	15
1.6 Objective of the present study.....	15
1.7 Thesis layout	15
References	17

Chapter II: Experimental techniques.....	19
2.1 Introduction.....	19
2.2 Solution combustion method	19
2.3 Characterization techniques.....	20
2.3.1 Scanning electron microscopy (SEM)	20
2.3.2 X-ray diffraction (XRD)	22
2.3.3 Photoluminescence (PL)	23
2.3.4 Energy Dispersive Spectroscopy (EDS)	24
2.3.5 Fourier Transform infrared spectroscopy (FTIR).....	25
References	27
Chapter III: Synthesis and characterization of SrAl₂O₄:Ce³⁺ phosphor using solution combustion method.....	28
3.1 Introduction.....	28
3.2. Experimental	29
3.2.1 Synthesis of SrAl ₂ O ₄ doped with Ce ³⁺	29
3.2.2 Characterization.....	31
3.3 Results and Discussion.....	31
3.3.1 X-ray diffraction	31
3.3.2 FTIR.....	32
3.3.3 Morphology	34
3.3.4 Photoluminescence spectra.....	35
3.4 Conclusion	39
References	40
Chapter IV: Synthesis and characterization of green SrAl₂O₄:Tb³⁺ phosphor using solution combustion method.....	41
4.1 Introduction.....	41

4.2 Experimental	42
4.3 Characterization	42
4.4 Results and Discussion	42
4.4.1 X-ray diffraction	42
4.4.2 Morphology	43
4.4.3 Photoluminescence (PL)	45
4.4.4 Decay curves and afterglow characteristics	47
4.5 Conclusion	49
References	50
Chapter V: Synthesis and characterization of a green $\text{CaAl}_x\text{O}_y:\text{Tb}^{3+}$ phosphor using solution combustion method.....	51
5.1 Introduction.....	51
5.2 Experimental procedure.....	52
5.3 Results and Discussion	52
5.3.1 Structure analysis of $\text{CaAl}_x\text{O}_y:\text{Tb}^{3+}$	52
5.3.2 Morphology of $\text{CaAl}_x\text{O}_y:\text{Tb}^{3+}$	54
5.3.3 Photoluminescence properties of $\text{CaAl}_x\text{O}_y:\text{Tb}^{3+}$	54
5.4 Conclusion	58
Reference.....	69
Chapter VI: Preparation and characteristics of $\text{Y}_3\text{Al}_5\text{O}_{12}:\text{Eu}^{3+}$ phosphor by solution combustion method.....	60
6.1 Introduction.....	60
6.2 Experimental Procedure	61
6.3 Results and discussion	61
6.3.1 X-ray diffraction and morphology.....	61
6.3.2 Photoluminescence	64

6.4 Conclusion	68
References	69
Chapter VII: General conclusion and summary.....	70
7.1 Thesis summary.....	70
7.2 Future work.....	72

List of Figures

Figure 1.1:	Three level model showing the mechanism of long persistent phosphorescence.....	2
Figure 1.2:	(a) A Fluorescence tube.....	5
Figure 1.2:	(b) Different types of commercially available fluorescence lamps.....	5
Figure 1.3:	Comparison chart for different types of commercially available fluorescent lamp.....	6
Figure 1.4:	A schematic diagram showing basic component of CRT.....	7
Figure 1.5:	A schematic diagram of flat panel TV's.....	8
figure 1.6:	Example of commeciarily available fluorescent absorbing UV and emitting light in the visible (a) and glowing in the dark (b).....	9
Figure 1.7:	Pictures of phosphorescent paint. A glow in the dark (a) statue of an eagle and (b) signs.....	10
Figure 1.8:	(a) Luminescence ion A in the host lattice, EXT: excitation, EM: emission, Heat: non radiative returns to ground state.....	11
Figure 1.8:	(b)Schematic energy level diagram of the luminescence ion A in the host lattice.....	11
Figure 1.9:	Different LCD device.....	12
Figure 1.10:	Different types of chemiluminescence: light sticks and a luminal test done on a bloody shoe print.....	13
Figure 1.11:	Land bioluminescence: (a) A firefly (b) the railroad worm (phrixothrix) is quite distinct for having two different colours of luminescent organs. Marine bioluminescence: (c) Image of bioluminescence showing brilliantly glowing	

	crashing waves (d) Tomopteris is a genus of marine planktonic polychaetes. These species emits light when disturbed.....	14
Figure 2.1:	Schematic diagram of SEM set-up.....	21
Figure 2.2:	Shimadzu Superscan SSX-550 SEM.....	21
Figure 2.3:	D8 advanced AXS GmbH X-ray diffractometer.....	23
Figure 2.4:	Cary Eclipse Photoluminescence Spectrophotometer equipped with a 150 W xenon lamp as the excitation source.....	24
Figure 2.5:	A simplified layout FTIR spectrometer.....	25
Figure 2.6:	Bruker TENSOR 27 Series FTIR spectroscopy.....	26
Figure 3.1:	Illustration of Monoclinic structure of SrAl_2O_4 ($P2_1$) with the linkage patterns of the $[\text{AlO}_4]$ tetrahedral. The closed gray circles indicate Sr atoms.....	29
Figure 3.2:	Flow diagram for the preparation of $\text{SrAl}_2\text{O}_4:\text{Ce}^{3+}$ phosphor.....	30
Figure 3.3:	XRD patterns of SrAl_2O_4 doped with different concentration of Ce^{3+}	31
Figure 3.4:	FTIR spectrum of $\text{SrAl}_2\text{O}_4:0.2\%\text{Ce}^{3+}$	32
Figure 3.5:	SEM images of $\text{SrAl}_2\text{O}_4:0.25\%\text{Ce}^{3+}$ (a) 1000x magnification (b) at magnification of 20000x. $\text{SrAl}_2\text{O}_4:1.5\%\text{Ce}^{3+}$ (c) at magnification of 1000x (d) at 20000x magnification. and $\text{SrAl}_2\text{O}_4:2\%\text{Ce}^{3+}$ (e) 1000x magnification and (f) 20000x magnification.....	33
Figure 3.6:	EDS spectra of $\text{SrAl}_2\text{O}_4:\text{Ce}^{3+}$	34
Figure 3.7:	Excitation spectra (a) emission spectra (b) of $\text{SrAl}_2\text{O}_4:\text{xCe}^{3+}$ and (c) Ce^{3+} Expected Emission Spectrum.....	35
Figure 3.7:	(c) Shows Ce^{3+} expected emission spectrum.....	36
Figure 3.8:	Maximum PL intensity as a function of Ce^{3+}	37
Figure 3.9:	Decay curves of $\text{SrAl}_2\text{O}_4:\text{Ce}^{3+}$ phosphor with different Ce concentrations 0.25 mol%(a) 0.4 mol% (b) 0.5 mol% (c) 0.7 mol% (d) and 1.5 mol% (e)....	38

Figure 4.1:	XRD patterns of SrAl ₂ O ₄ : Tb ³⁺ with different concentration of terbium.....	43
Figure 4.2:	SEM image of SrAl ₂ O ₄ : 0.4% Tb ³⁺ (a) and SrAl ₂ O ₄ : 0.5% Tb ³⁺ (b) at 1000x magnification.....	44
Figure 4.3:	EDS spectrum of SrAl ₂ O ₄ : 0.5% Tb ³⁺	45
Figure 4.4:	Excitation spectra of SrAl ₂ O ₄ :Tb ³⁺ with different concentration of Tb ³⁺ . λ _{em} =543.....	46
Figure 4.5:	Emission spectra of SrAl ₂ O ₄ :Tb ³⁺ with different concentration of Tb ³⁺ . λ _{ex} =229.....	46
Figure 4.6:	Graph of concentration dependence of the emission maximum intensity of Tb ³⁺ doped SrAl ₂ O ₄	46
Figure 4.7:	Decay curves of SrAl ₂ O ₄ :Tb ³⁺ of different concentration of terbium Tb ³⁺	48
Figure 4.8:	Mechanism of SrAl ₂ O ₄ :Tb ³⁺ phosphor.....	48
Figure 5.1:	X-ray diffraction patterns of CaAl _x O _y with different concentrations of Tb ³⁺	53
Figure 5.2:	FTIR spectra of CaAl _x O _y : Tb ³⁺ phosphor (a) 0.4 mol% and (b) 1.5 mol%.....	53
Figure 5.3:	SEM image of CaAl _x O _y : Tb ³⁺ phosphor (a) 2 mol% and (b) 1.5 mol% at 1000x magnification.....	54
Figure 5.4:	EDS spectra of CaAl _x O _y : Tb ³⁺ with different concentration of Tb ³⁺	55
Figure 5.5:	(a) Photoluminescence excitation and (b) emission spectra of CaAl _x O _y : Tb ³⁺ (c) PL maximum intensity as a function of Tb ³⁺ concentration.....	56
Figure 5.6:	Decay curves of CaAl _x O _y : Tb ³⁺ phosphor for different Tb ³⁺ concentration as indicated.....	57
Figure 6.1:	XRD pattern of Y ₃ Al ₅ O ₁₂ :Eu ³⁺ phosphor.....	62
Figure 6.2:	SEM photographs of Y ₃ Al ₅ O ₁₂ :Eu ³⁺ phosphor doped 0.4 mol% (a) 0.4 mol% (b) and 1.4 mol% (c) of Eu ³⁺ respectively.....	63
Figure 6.3:	FTIR spectra of Y ₃ Al ₅ O ₁₂ :Eu ³⁺ phosphor.....	63

Figure 6.4:	EDS spectra of $Y_3Al_5O_{12}:Eu^{3+}$	64
Figure 6.5:	Excitation spectra of $Y_3Al_5O_{12}:Eu^{3+}$ phosphor with different concentration of Eu^{3+}	65
Figure 6.6:	Emission spectra of $Y_3Al_5O_{12}:Eu^{3+}$ phosphor with different concentration of Eu^{3+}	65
Figure 6.7:	PL maximum intensity as a function of Eu^{3+} concentration.....	66
Figure 6.8:	Decay curves of $Y_3Al_5O_{12}:Eu^{3+}$	67

List of Tables

Table 1:	The estimated average particle sizes of $SrAl_2O_4$ doped Ce^{3+}	32
Table 2:	Decay parameters of the $SrAl_2O_4:Ce^{3+}$ samples with different doped Ce concentrations.....	38
Table 3:	Particle sizes for $SrAl_2O_4:xTb^{3+}$ ($x=2, 1, 0.5$ and 0.4%) phosphor.....	43
Table 4:	Decay parameters of the $SrAl_2O_4:Tb^{3+}$ phosphor with different Tb^{3+} concentration.....	49
Table 5:	Decay parameters of the $SrAl_xO_y:Tb^{3+}$ phosphor with different Tb^{3+} concentration.....	57
Table 6:	Decay parameters of the $Y_3Al_5O_{12}:Eu^{3+}$ phosphor with different Eu concentration.....	67

Chapter I

General Introduction

1.1 Phosphor terminology and definition of phosphor

The term phosphor was invented in the early 17th century in Italy by an Italian alchemist, Vincentinus Casciarolo when he fired the Bolognian stone or Litheophosphorus in an oven to obtain gold [1]. The sintered stone was found to emit red light in the dark after exposure to sunlight. This marked the first object of scientific study of luminescence phenomena. Current knowledge has now established that the Bologna stone was BaSO_4 and the fired product was BaS ($\text{BaSO}_4 + 2\text{C} \rightarrow \text{BaS} + 2\text{CO}_2$) which is a host for phosphor materials. Later phosphor developments occurred in 1768 when Canton obtained CaS and then in 1866 when Sidot formed the first ZnS, green emitting luminescent material. In 1886 Verneuil proved that pure CaS did not luminesce and the trace of Bi was necessary for light emission and that is when the understanding of these materials began. It was found that a trace of Cu was necessary for emission from green ZnS and Cr for red BaS [1].

In general, a phosphor material is a substance that absorbs energy in the form of photons and undergoes radiative recombination to emit visible light. The word phosphorescent was also derived from the word phosphor and it means the persisting light emission from a substance after the excitation source has ceased. Fluorescence on the other hand refers to light emission from a substance during exposure to an excitation source. The term Luminescence, which includes both fluorescence and phosphorescence, is the radiative recombination of the excited electrons and holes to emit light at varying wavelengths [1].

1.2 Long persistent phosphors (LPP)

Long persistent phosphors, also called long lasting or long afterglow phosphors are phosphors that have a very long afterglow emission or phosphorescence, even longer than a whole day in some cases [3]. The electrons that are trapped or holes that are produced during excitation cause the afterglow.

Mechanism of long persistent glow or phosphorescence can be explained with the aid of an electronic energy diagram which includes the ground state, an excited state and meta-stable deep trapping state for active electron (figure 1.1).

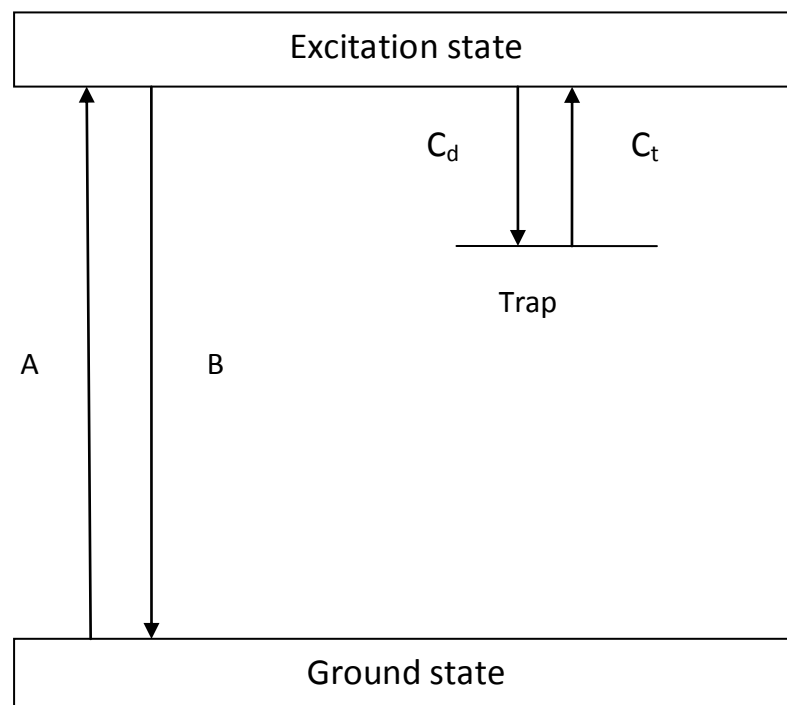


Figure 1.1: Three level model showing the mechanism of long persistent phosphorescence [3]

As shown in figure 1.1 C_t and C_d are the trapping and de-trapping rates respectively, while A and B represent the excitation and emission rates respectively. Phosphorescence life times are usually depended on the trap depth, trapping and de-trapping rates and are therefore longer than the life times of the excited state [3]. On the other side fluorescence is based on the two level electron transition mechanism, ground and excitation state and its decay time depend on the transition strength between the two states.

Phosphorescence is classified according to its life time as: very short persistence phosphorescence (VSPP) that has life time of the same order of magnitude as the life time of excited state, that is in the order of milliseconds and is associated with very shallow traps. Short persistence phosphorescence (SPP) that lasts for few seconds, and become noticeable by human eyes. Most phosphor shows short persistent phosphorescence after exposure to UV, visible light, plasma beam or X-rays. Persistence phosphor that last for minutes is due to the deep traps in the materials.

1.2.1 Methods to design Long Persistent Phosphor (LPP)

The persistent time of a practical applications afterglow emission is of the most interest. However there are many factors that have to be considered like efficiency, emission color, chemical and physical stability, quenching effects, reproducibility of material preparation and properties, availability of raw materials, environmental aspects, and cost factors. Persistent time has been increased by developed methods by producing more traps in the host and by increasing trapping-detrapping efficiency. Some of these are discussed below.

1.2.1.1 Co-doping

One of the most commonly used method to make long persistent phosphors is co-doping. The co-doping ions serve as trap centers or produce defect related trapping centers when introduced into host. The persistent time can be significantly increased with the introduction of proper codopants [4]. Example Mg^{2+} and Ti^{4+} are doped into $\text{Y}_2\text{O}_2\text{S}:\text{Eu}^{3+}$ to replace Y^{3+} [5], Cl^- ion is doped into CaS to replace S^{2-} [6]. Some ions act as trapping centers when co-doped into the host. These ions trap either the electrons or holes and converted into meta-stable ionic states. Typical examples of these types include

- $\text{CaAl}_2\text{O}_4:\text{Eu}^{2+}/\text{Nd}^{3+}$
- $\text{SrAl}_2\text{O}_4:\text{Eu}^{2+}/\text{Dy}^{3+}$ [7].

The consequence of co-ion co-doping is not only to create an extra trap centers in the host but also enhance the trapping efficiency. Therefore larger trap population can be attained by using ions with stronger transition rates which push electrons more efficiently in the conduction band. An example is Ce^{3+} doped MgAl_2O_4 where electrons are pumped into the traps through Ce^{3+} 4f-5d transitions that populate traps 30 times more than those populated through host band gap absorption [8].

1.2.1.2 Persistent energy transfer

In persistent energy transfer, the emission center of a known long persistent phosphor is used as the donor and the choice of acceptor is based on its color. The choice of the acceptor ion depends on the presence of the absorptions at the donor emission frequency to support the emission by the acceptor. The energy difference between the ground and excited states of donor and acceptor should be in resonance condition for energy transfer to occur and also suitable interaction of either exchange of electric or magnetic multipolar interactions between ions should be possible. The acceptor absorption spectra should be overlapped by the donor emission spectra. The traps continuously transferring energy to support the emission by the acceptor, and these traps are associated with the donor when charged [8]. Long persistence of donor is converted into the long persistence of acceptor at the required frequency. This method has been found effective in preparing long persistent phosphors. An example of persistent energy transfer is $\text{CaAl}_2\text{O}_4: \text{Tb}^{3+}/\text{Ce}^{3+}$, where persistence time of Ce^{3+} afterglow last longer than 10 h while that of Tb^{3+} persists for about 1 h, and energy has been successfully transferred to yield 10 h green Tb^{3+} [9].

1.2.1.3 Doubly doped materials

Mixing two or more persistent phosphors constitutes another method to obtain long persistence at desired colors. This can result in time dependent emission color changes because of the variations in the persistent times of the components. For this to happen, multiple emission centers can be doped into the same host in the hope that the decay times are equalized by the same detrapping mechanism. Eu^{2+} and Bi^{3+} doped CaS is an example of material produced by this method. The mixing of Eu^{2+} (red) and Bi^{3+} (blue) yields long persistent afterglow emission with a stable purplish red color due to the similar afterglow decay mechanism of these two ions [10].

Another method involves the substitution of the host material with a single elemental dopant.

Typical example include

- Replacing Sr with Ca in the $\text{SrAl}_2\text{O}_4:\text{Eu}^{2+}/\text{Dy}^{3+}$ to produce bluish green afterglow, which is attributed to the mixing of $\text{CaAl}_2\text{O}_4:\text{Eu}^{2+}/\text{Dy}^{3+}$ (Blue) and $\text{SrAl}_2\text{O}_4:\text{Eu}^{2+}/\text{Dy}^{3+}$ (Green).
- Similarly, substitution of Ba by Sr causes the blue shift in the $\text{BaAl}_2\text{O}_4:\text{Eu}^{2+}/\text{Dy}^{3+}$ [8].

1.3 Applications of phosphors

1.3.1 Fluorescent lamp

Because of their usefulness, fluorescent lamps come in many sizes, types, shapes, colors and light intensity [11]. Fluorescent lamp converts electrical power into useful light. Fluorescent lamps give off light by discharging an electrical current through a fluorescent tube. A fluorescent tube contains an inert gas filled with a tiny amount of mercury vapor. Ultraviolet radiation is produced as the electrons of the atoms in the electric current strikes electrons of the mercury atoms and the mercury electron will jump to a higher energy level in the atom and then immediately return to its original level. The phosphor coating inside the fluorescent lamp converts the ultraviolet radiation into visible light.

The electric current through the fluorescent is provided by ballast which limit the amount of current required to operate the lamp

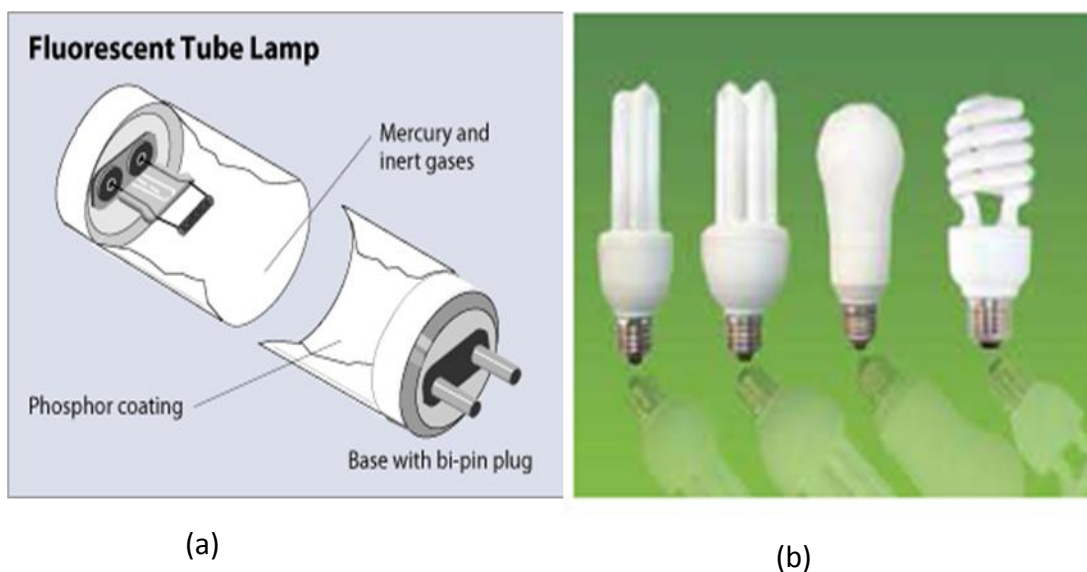


Figure 1.2: (a) A fluorescence tube [12] (b) Different types of commercially available fluorescent lamps [13]

Fluorescent Lighting Comparison

Fluorescent lighting type	Efficacy (lumens/Watt)	Lifetime(hours)	Color Rendition Index (CRI)	Color Temperature (K)	Indoors/outdoors
Straight tube	30-110	7000-24,000	50-90 (fair to good)	2700-6500 (warm to cold)	Indoors/outdoors
Compact fluorescent lamp (CFL)	50-70	10,000	65-88 (good)	2700-6500 (warm to cold)	Indoors/outdoors

Figure 1.3: Comparison chart for different types of commercially available Fluorescent lamp [14]

1.3.2 Cathode ray tube (CRT)

Almost all TVs in use today rely on a device called a cathode ray tube to display their images [15]. CRT is a vacuum tube containing an electron gun (source of electrons) and a fluorescence screen. The cathode is a heating filament that emits a beam of electrons in the vacuum which are accelerated by the anode towards the phosphor screen [15]. The screen is coated with a phosphor. Deflection coils produce magnetic fields that control the direction of electron beam. There are two types of deflection coils: horizontal and vertical deflection coils. Combination of these two deflections allows the beam to reach any portion of screen. When the beam of electrons strikes the screen, the phosphor is excited and light is emitted from that point [16, 17]. CRTs can be used in oscilloscopes, television, computer monitors and others.

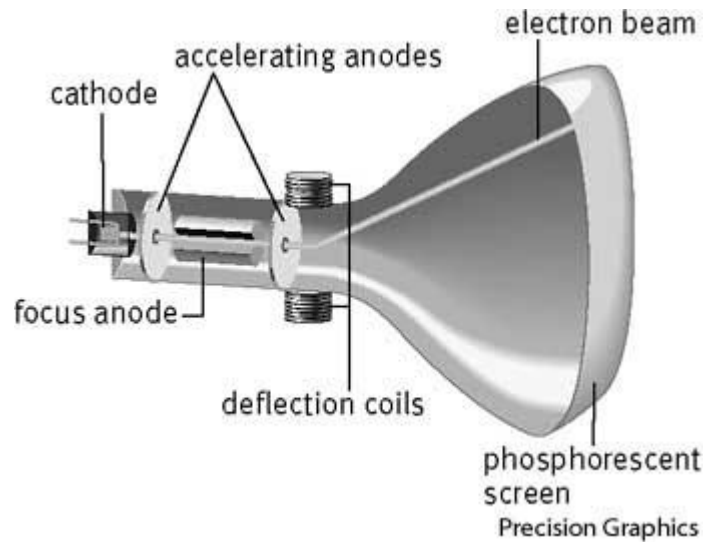


Figure 1.4: Schematic diagram showing basic component of CRT used in television and computers [18]

1.3.3 Flat panel display (FPD)

Flat panel display (sometimes known as flatscreen) encompass a growing number of technologies like liquid crystal displays (LCD) that compare much lighter and thinner with traditional television sets and video displays that use cathode ray tubes (CRT). They are usually less than 100 mm thick. In FPD a small amount of power to accelerate the electrons from anode to the cathode. They have a high contrast and high resolution and have excellent color range. They can be used in many applications, especially modern portable devices such as laptops, cellular phones, digital cameras and compact cameras [19]. FPLs have many examples such as:

- Electroluminescence displays (ELDs)
- Digital light processing (DLP)
- Field emission displays (FEDs)
- Light-emitting diode displays (LED)
- Liquid crystal displays (LCDs)
- Organic light-emitting diode (OLED)
- Surface-conducting electron-emitter displays (SEDs)
- Plasma display panels (PDPs)



Figure 1.5: Schematic diagram of flat panel TV's [19]

1.3.4 Other applications

1.3.4.1 Luminescent paints

Luminescent paints are paints that exhibit luminescence and are suitable for various applications. They can be subdivided into two forms depending on the nature of their glow:

- Fluorescence paints are characterized by glowing in the light, while
- Phosphorescent paints on the dark.

In addition, the mixing of crystalline luminescent with radioactive material forms radioluminescent paints which have been predominantly used in the past on clocks, watches, compass, toys, fish baits, weapon aiming site etc. However, the scope of their application is constrained by its radioactive nature.

1.3.4.1.1 Fluorescent paint

Fluorescent paints are widely used in the industrial manufacture of marking materials/pigment. Fluorescent paint reacts to long-wave ultraviolet radiation known as black light. Sensitive pigment present in the fluorescent paints absorbs UV light to emit in the visible range high brilliant glow in the dark. This paint is available in many colors, the most common are yellow, green, orange and red. Fluorescent paint can be either water-based or solvent based [20]. The fluorescent paint can be applied to a variety of substrates such as textile, paper, wood, coated metal and some plastics. Example of fluorescent paint is shown in figure 1.6.



(a)

(b)

Figure 1.6: Example of commercially available fluorescent absorbing UV and emitting light in the visible (a) and glow in the dark (b) [21].

1.3.4.1.2 Phosphorescent paint

Phosphorescent paint (glow in the dark) is made from phosphors and is also used for markings and signage. Phosphorescent paints have been successfully applied in safety, novelty and industrial applications. The pigments or paints that glow in the dark have to be charged with light. The pigment in phosphorescent paint absorbs the light and emits it. The emission of the visible light persists for some time after it has been absorbed. Some toys, road signs, house numbers and wall-coverings coated with phosphorescent paint glow in the dark. These are materials that contain phosphorescent pigments such as zinc sulfide [20].



(a)

(b)

Figure 1.7: Pictures of phosphorescent paint. A glow in the dark (a) statue of an eagle and (b) signs [22, 23]

1.4 Fundamentals of luminescence

The type of excitation sources determines the nature of Luminescence. Accordingly several types of luminescence are identified, namely

- Photoluminescence where excitation is by means of electromagnetic radiation/photons
- Cathodoluminescence by energetic electrons
- Electroluminescence by electric voltage
- Chemiluminescence by the energy of chemical reaction
- Bioluminescence by living organism, etc.

A discussion of these types is provided below

1.4.1 Photoluminescence

Photoluminescence is a process in which a photon is absorbed by bound electrons to produce an exciton which decays through radiative recombination to emit light [24].

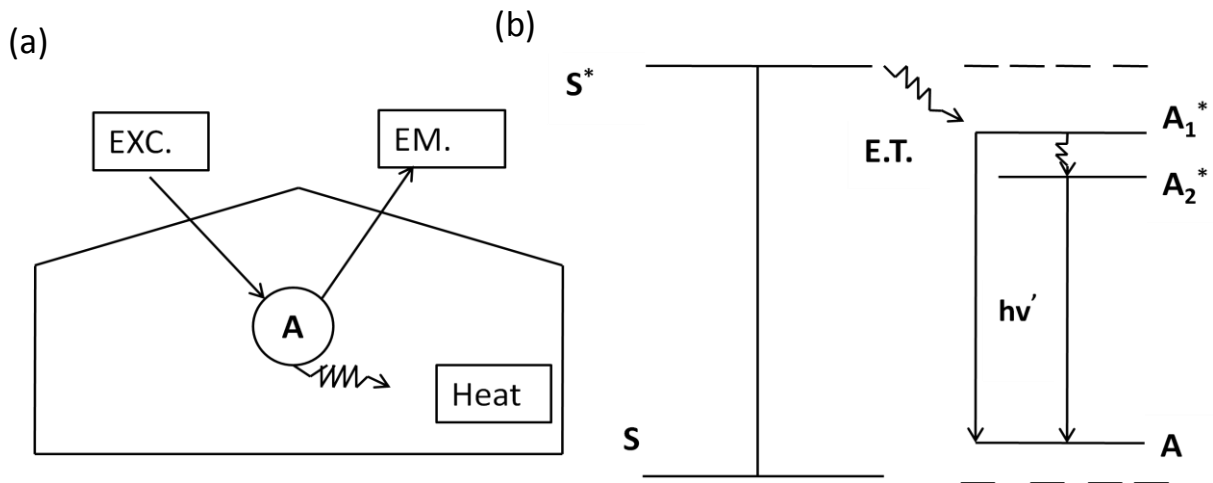


Figure 1.8: (a) Luminescence ion A in the host lattice, EXT: excitation, EM: emission, Heat: non radiative returns to ground state and (b) Schematic energy level diagram of the luminescence ion A in the host lattice [8]

Figure 1.8 illustrates a simple luminescence system comprising of an activator ion (A). This ion absorbs exciting radiation which raises it to the excitation state (A*). The excited state can return to the ground state in two possible ways:

- (i) By radiative emission also known as luminescence
- (ii) By nonradiative process or transition in which the energy is transferred as phonons to excite lattice vibrations of the host

Typical examples of the luminescence system include:

$\text{Al}_2\text{O}_3:\text{Cr}^{3+}$ where Al_2O_3 is the host and the activator is Cr^{3+} ion, in above context: Cr^{3+} absorbs the excitation energy to transit to the excited state (Cr^{3+})*. The transition back to the ground state leads to the emission of red light in the dark [8].

1.4.2 Cathodoluminescence

Cathodoluminescence is an opto-electrical phenomenon in which a beam of electrons impacts a luminescent material to emit light. The impacting electrons cause electrons from the luminescence material to be promoted from the valence band to the conduction band and thereby created a hole in the valence band. Electron-hole recombination leads to the emission of light photons whose energy is determined by the electronic structure of the materials (Band

gap), its purity and nature of defects in it. Cathodoluminescence is mostly performed in the scanning electron microscope.

1.4.3 Electroluminescence

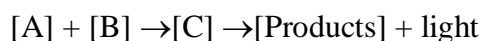
Electroluminescence is an electro-optical phenomenon in which light is emitted by a material as a result of the application of an electric current or strong electric field. The energy of the excited electron is released as a photon (light). Prior to recombination, electrons and holes can be separated either by doping material to form a p-n junction (in semiconductor electroluminescent devices such as LEDs) or through excitation by impact of high energy electrons accelerated by strong electric field (as with the phosphors in electroluminescent displays). Examples of electroluminescence include zinc sulphide (ZnS) doped with Cu, ZnS doped with Mn, natural blue diamond (diamond with boron as dopant). The backlights are powder phosphor-based electroluminescent panels and are used in liquid crystal displays. They readily provide a gentle, even illumination to the entire display while consuming relatively little electric power. This makes them convenient for battery-operated devices such as wristwatches, pagers, and computer-controlled thermostats. Different LCD device is shown in figure 1.9.



Figure 1.9: different LCD device [24, 25]

1.4.4 Chemiluminescence

Chemiluminescence is the emission of light from de-excited electrons after a chemical reaction. The energy used to excite the electrons is released from a chemical reaction. Given reactants A and B with an excitation intermediate C,



If [A] is luminal and [B] is hydrogen peroxide in the presence of a suitable catalyst we have,
 $\text{luminal} + \text{H}_2\text{O}_2 \rightarrow 3\text{-APA}[C] \rightarrow 3\text{-APA} + \text{light}$

Where 3-APA is 3-aminophthalate, 3-APA[C] is the excited state fluorescing as it decays to a lower energy level. The decay of the excited state [C] to a lower energy level is the source of the emitted light. In theory, one photon of light should be given off for each molecule of reactant and is equivalent to Avogadro's number of photons per mole of reactant. One example of chemiluminescence is the luminal test, where luminal is used in conjunction with H_2O_2 and KOH as a forensic detector to detect trace elements of blood. Liminol ($\text{C}_8\text{H}_7\text{O}_3\text{N}_3$) reacts with Fe found in haemoglobin as a catalyst for the chemiluminescent reaction which emits a blue glow lasting for approximately 30 seconds. A light stick emits a form of light by chemiluminescence [26].

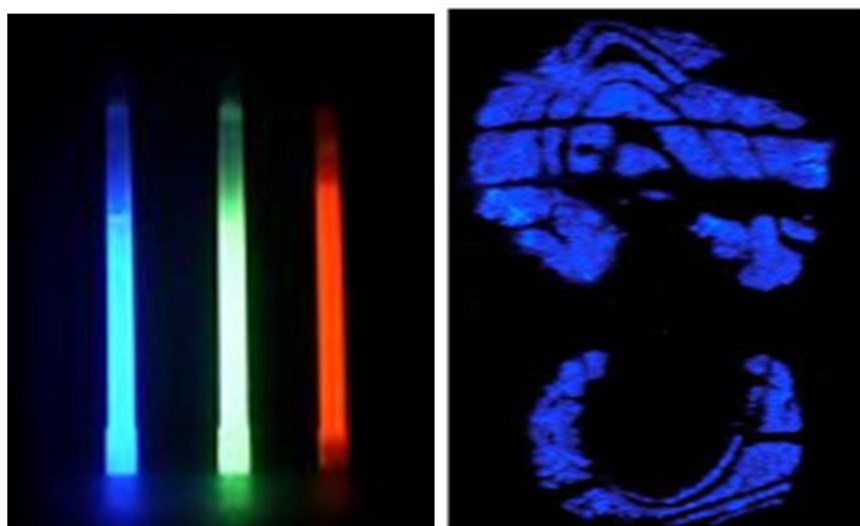


Figure 1.10: Different types of chemiluminescence: light sticks [27] and a luminal test done on a bloody shoe print [28].

1.4.5 Bioluminescence

Bioluminescence is a kind of chemiluminescence in which the chemical reaction involved takes place within a living organism. It is the emission of light by a living organism [29]. Chemical within the organ such as *Luciferin* reacts with oxygen in the presence of catalyst, *Luciferase* to produce light. The chemical reaction can occur either inside or outside the cell [29]. Bioluminescence occurs in marine vertebrates and invertebrates, as well as microorganisms and terrestrial animals. Ninety percent of deep-sea marine life is estimated to produce bioluminescence in some form. Most of the light created by marine organisms is blue-green in color. This is because blue light travels best in water, and because most of marine organisms are sensitive to blue light. Non-bioluminescence is less widely distributed, but they display a larger variety of colours. The best-known forms of land bioluminescence are fireflies and glow worms. Figure 2.1 show forms of marine and land bioluminescence.

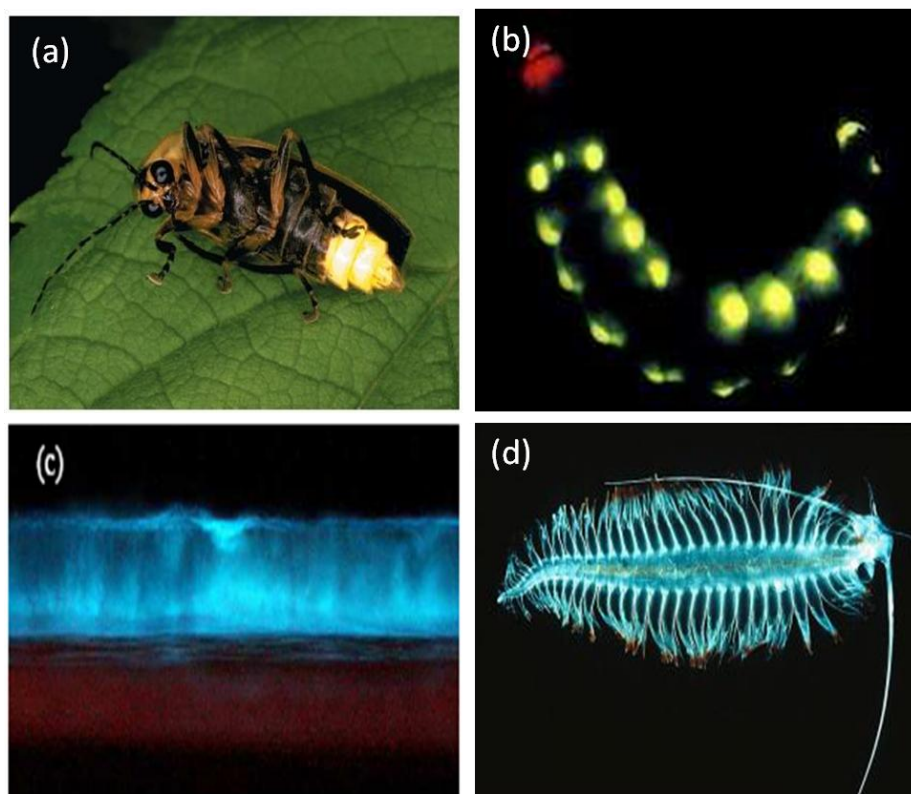


Figure 1.11: Land bioluminescence: (a) A firefly [29] (b) the railroad worm (*Phrixothrix*) is quite distinct for having two different colours of luminescent organs [30]. Marine bioluminescence: (c) Image of bioluminescent showing brilliantly glowing crashing waves [31] (d) *Tomopteris* is a genus of marine planktonic polychaetes[32]. These species emit light when disturbed

1.5 Statement of problem

ZnS has been well known as a long lasting phosphor with applications in a wide range of industries, however it did not show sufficient brightness and long lasting phosphorescence. In the past decade long persistent phosphors were invented. Aluminate phosphors due to their several advantages over other phosphors have widely been investigated. Rare earth doped aluminate phosphors are widely used in display and lighting applications because of their good luminescent properties.

In the present study the phosphors doped with different concentrations of rare earth ions ($\text{SrAl}_2\text{O}_4:\text{Ce}^{3+}$, $\text{SrAl}_2\text{O}_4:\text{Tb}^{3+}$, $\text{CaAl}_x\text{O}_y:\text{Tb}^{3+}$ and $\text{Y}_3\text{Al}_5\text{O}_{12}:\text{Eu}^{3+}$) were investigated. These phosphors are promising materials in the field of luminescent materials. The effect, structure and optical properties of different concentrations of rare earths on the phosphor matrix will also be investigated.

1.6 Objective of the present study

- To prepare and characterize the alkaline earth aluminate phosphors activated with rare earth ions
- To investigate the luminescent properties of rare earths activated alkaline earth aluminate phosphor materials prepared by solution combustion method.
- To investigate the effect of different concentration of rare earths on the structural and luminescent properties of the long persistent phosphors ($\text{SrAl}_2\text{O}_4:\text{Ce}^{3+}$, $\text{SrAl}_x\text{O}_y:\text{Tb}^{3+}$, $\text{CaAl}_2\text{O}_4:\text{Tb}^{3+}$, $\text{Y}_3\text{Al}_5\text{O}_{12}:\text{Eu}^{3+}$).

1.7 Thesis layout

A summary of the contents in each chapter of this thesis is provided below

Chapter 2 describes briefly the experimental techniques used to synthesize and characterize phosphors. This chapter includes a detailed description of the systematic procedure used to synthesize phosphors using solution combustion method. A brief description of the working principle for each technique is discussed.

Chapter 3 discusses the results on photoluminescence properties (PL), structural properties (XRD), morphology (SEM), elemental composition (EDS) and chemical bond (FTIR) of $\text{SrAl}_2\text{O}_4:\text{Ce}^{3+}$.

In chapter 4 and chapter 5 the different concentration of Tb^{3+} in $\text{SrAl}_2\text{O}_4:\text{Tb}^{3+}$ and $\text{CaAl}_x\text{O}_y:\text{Tb}^{3+}$ phosphors are discussed. In addition, the effect of Tb^{3+} concentration on the crystal structure, photoluminescence and luminescence lifetimes of the phosphors are presented and discussed.

Chapter 6 presents in detail the results of red emitting $\text{Y}_3\text{Al}_5\text{O}_{12}:\text{Eu}^{3+}$ phosphors prepared by the solution combustion method.

Lastly, the summary and conclusion of this thesis together with the suggestions for future work are presented in chapter 7.

References

- [1] http://www.isbc.unibo.it/Files/10_SE_BoStone.htm [Accessed 26 November 2011]
- [2] P.A Moleme, Msc. Dissertation, University of the Free State, (2011)
- [3] N. Alcon, A. Tolosa, M. Pico, I. Inigo, Wiley Periodical, Inc., **36**, No 5, (2011)
- [4] M. Ohta, M. Takami, Journal of Electrochemical Society, **151**(2), G171-G174. (2004)
- [5] Y. Li, Y. Wang, Y. Gong, X. Xu, M. Zhou, Optics express 24853, **18**, No. 24, (2010)
- [6] D. Jia, X. J. Wang, E. van der Kolk, W. M. Yen, Optics Communications, **204**, 247-251. (2002)
- [7] http://violet.vn/vanhuy_06/document/showprint/entry_id/2705198 [Accessed 26 November 2011]
- [8] N. H Luitel, Phd. dissertation, Science and Engineering Saga University, (2010)
- [9] D. Jia, X. J. Wang, W. Jia, W. M. Yen, Journal of Applied Physics, **93**, No1, (2003)
- [10] J. Dongdong, W. Bo-Qun, Z. Zing, L. Acta Physica Sinica, **8**, No. 11, (1999)
- [11] <http://nemesis.lonestar.org/reference/electricity/fluorescent/lamps.html> [Accessed 3 September 2011]
- [12] <http://www.eere.energy.gov/basics/buildings/fluorescent.html> [Accessed 26 November 2011]
- [13] <http://kushweed.blogspot.com/2011/05/how-do-you-replace-fluourescent-light.html> [Accessed 28 November 2011]
- [14] http://www.energysavers.gov/your_home/lighting_daylighting/index.cfm/mytopic=12040 [Accessed 28 November 2011]
- [15] <http://electronics.howstuffworks.com/tv3.htm> [Accessed 28 November 2011]

- [16] <http://searchcio-midmarket.techtarget.com/definition/cathode-ray-tube> [Accessed 28 November]
- [17] <http://www.physics.sc.edu/~hoskins/Demos/CathodeRay.html> [Accessed 16 September 2011]
- [18] <http://mypcmag.com/2010/11/cathode-ray-tube/> [Accessed 26 November 2011]
- [19] http://en.wikipedia.org/wiki/Flat_panel_display
- [20] <http://greatpaintingtips.com/fluorescent-paint-vs-luminous-paint/2008/06/01/> [accessed 23 September 2011]
- [21] <http://www.manufacturer.com/business/search?isnew=all&type=SellLeads&arg=o243&keywords=Paint&start=31> [Accessed 28 November 2011]
- [22] <http://en.wikipedia.org/wiki/Phosphorescence>
- [23] <http://www.glonation.com/signs-and-tape.html> [Accessed 29 November 2011]
- [24] <http://www.diytrade.com/china/4/products/3223048/CALCULATOR.html> [Accessed 29 November 2011]
- [25] <http://www.amazon.com/Casio-AQ160W-1BV-Ana-Digi-Electro-Luminescent-Sport/dp/B000GB0FYO> [Accessed 29 November 2011]
- [26] <http://en.wikipedia.org/wiki/Chemoluminescence>
- [27] <http://www.jce.divched.org/JCESoft/CCA/CCA3/MAIN/ILUMIN/PAGE1.HTM> [Accessed 30 November 2011]
- [28] M. M. Biggs, Msc. dissertation, University of the Free State, (2009)
- [29] <http://www.scienceclarified.com/Io-Ma/Luminescence.html#ixzz1WjnJ33GC> [Accessed 30 November 2011]
- [30] <http://www.lifesci.ucsb.edu/~biolum/forum/vviviani2.html> [Accessed 29 November 2011]
- [31] <http://www.newworldencyclopedia.org/entry/Bioluminescence> [Accessed 26 November 2011]
- [32] <http://tinylittleanthill.wordpress.com/2010/03/19/deep-sea-bioluminescence-2/> [Accessed 4 October 2011]

Chapter II

Experimental techniques

2.1 Introduction

In this chapter, the theoretical background of the experimental techniques used to synthesize and characterize alkaline based aluminates is given. The solution combustion method was used to synthesize alkaline aluminate phosphors. Synthesized powders that were investigated in this study were characterized using x-ray diffraction (XRD), scanning electron microscopy (SEM) and energy dispersive spectroscopy (EDS), to investigate the crystal structure, morphology and elemental composition of the phosphor. Photoluminescence (PL) was also used to investigate the emission and excitation properties and their corresponding decay characteristics. Last but not least a description on the Fourier transform infrared spectroscopy (FTIR) is provided to enable the identification of the types of chemical bonds.

2.2 Solution combustion method

The solution combustion method is a versatile, simple and rapid synthesis method for nanomaterials (eg, phosphor) using self sustained reaction in homogenous solutions of various oxidizers [1]. It has generated more interest in the field of nano-luminescence materials.

The solution combustion method has been carried out using urea ($\text{CH}_4\text{N}_2\text{O}$), glycine ($\text{C}_2\text{H}_5\text{NO}_2$) and carbonhydrazides ($\text{CH}_6\text{N}_4\text{O}$) as fuel. It is an exothermic process that occurs with the evolution of heat. The energy needed for the combustion reaction to take place is supplied from the reaction itself hence it is called a self-propagating high-temperature synthesis [2, 3]. The characteristics of solution combustion reaction, to reduce power and

generate gas and can be controlled by the selection of the fuel such as $\text{CH}_4\text{N}_2\text{O}$, $\text{C}_2\text{H}_5\text{NO}_2$ and $\text{CH}_6\text{N}_4\text{O}$. Compared to other conventional ceramic process technique solution combustion method has shown advantages of taking few seconds to complete the reaction and the equipment processing are inexpensive [1].

2.3 Characterization techniques

2.3.1 Scanning electron microscopy (SEM)

Scanning electron microscopy is a technique that uses high energy beam of electrons to form an image. SEM has large depth of field (30 mm), a high resolution (1.5 nm) and a magnification (10x-500Kx) much higher than that of an ordinary optical microscope. Topographical and morphological studies are carried out by scanning an electron probe across a surface and monitoring the secondary electron emitted. Electron-specimen interaction produces x-rays characteristics to the specimen thereby enabling composition analysis [4].

The lanthanum hexaboride (LaB_6) filament is heated by an applied voltage to emit a beam of electrons which are accelerated towards the sample by a series of successive electric potentials applied to the lenses. The electron beam is focused and rastered over the sample by an objective lens and Magnetic scanning coils (Helmholz coils). Electrons in the sample absorb energy when the primary electrons strike the sample, and are emitted as secondary electrons. These secondary electrons have lower energies (20eV) and are collected by an Everhart Thornley detector. Detected electrons are converted to a signal used to generate the image on the CDT screen. The sample placed in SEM must be either conducting or coated with a thin metal layer to avoid sample charging. Schematic layout of atypical SEM is shown in figure 2.1.

The morphologies of the phosphor powders were obtained by using a Shimadzu Superscan SSX-550 SEM.

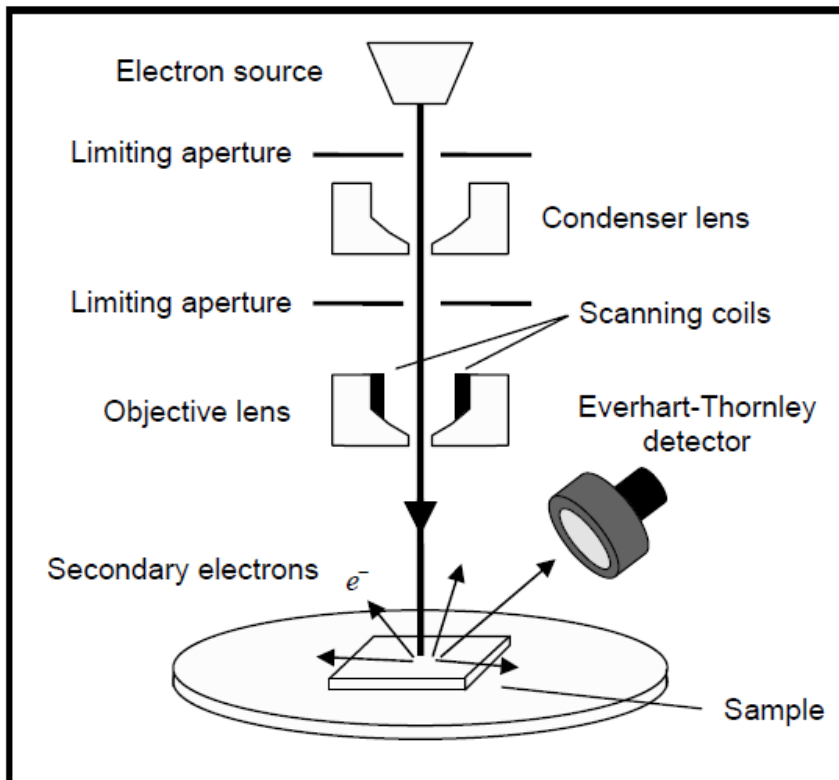


Figure 2.1: Schematic diagram of SEM set-up [4]



Figure 2.2: Shimadzu Superscan SSX-550 SEM

2.3.2 X-ray diffraction (XRD)

X-ray diffraction technique is the most common and efficient method for the determination of structure, crystallinity and material identification. This non-destructive technique is appropriate for phase identification of major constituents in a mixture. In addition, it can also be used to determine the lattice constants, macro stress or macro strain in solid solutions as well as the chemical composition of constituent phase in a material [5, 6].

A typical diffraction pattern comprises of peak positions and their corresponding intensities, these provide information about the size of the unit cell and also on the arrangement of atoms in the unit cell. The peak intensity is determined by the atomic position in the reciprocal space as well as the form factors of the constituent atoms. Phase identification is attained through comparison with a reference database. The sharp diffraction peaks are characteristic of crystalline materials with long range translational order. Disordered solids or amorphous material yield broad peaks indicative of the existence of local order. In some instances, small sized crystallites or nano-materials lead to peak broadening. The peak broadening can be used to determine the average crystalline size based on the Decay-Scherrer expression:

$$d = k\lambda/\beta\cos\theta \quad (2.1)$$

Where d is the average size of the crystallites, k is a Scherrer constant ≈ 0.9 , λ is the x-ray wavelength, β is the broadening of the diffraction line measured at half the maximum intensity in radians, and θ is the Bragg angle. The D8 Advanced AXS GmbH X-ray diffractometer, equipped with Cu $K\alpha$ radiation shown on figure 3, from University of the Free State was used to analyze the sample in this study.



Figure 2.3: D8 advanced AXS GmbH X-ray diffractometer

2.3.3 Photoluminescence (PL)

Photoluminescence spectroscopy is a contactless and nondestructive method of probing the electronic properties of materials [7]. Photoluminescence light emission can be used to yield information about the photoexcited material. Electronic energy levels can be determined by transition energies of a PL spectrum [8].

The sample's PL emission properties can be characterized by four parameters: intensity, emission wavelength, bandwidth of the emission peak and the emission stability [4]. PL intensity and spectral content is a measure of various important material properties like chemical composition, structure, impurities, kinetic process and energy transfer [9].

In this study a Cary Eclipse Fluorescence Spectrophotometer (shown in figure 2.4) coupled with a monochromator xenon lamp was used to collect fluorescence data. The photoluminescence excitation and emission spectra as well as exponential decay times of the alkaline earth aluminates phosphor powders were determined.



Figure 2.4: Cary Eclipse Photoluminescence Spectrophotometer equipped with a 150 W xenon lamp as the excitation source

2.3.4 Energy Dispersive Spectroscopy (EDS)

Energy dispersive x-ray spectroscopy is the technique that determines the elemental composition of small objects or surface [10]. It can also be used to identify unknown material found during production. EDS is non-destructive and has a sensitivity of $>0.1\%$ for elements heavier than C [11].

High energy beams of charged particles such as electrons are focused on the sample. The atoms in the sample originally in the ground state are excited by electrons to produce characteristic x-rays [11, 12]. The nature of the characteristic X-ray depends on

- The inner shell at which the electron is excited
- The transition from the outer shell based to the created hole based on the selection rules of the transition and the fluorescent yield of the level.

EDS systems are most commonly found on Scanning Electron Microscopes (SEM-EDS) and the EDS used in this study is seen in Figure 2.2. A detector is used to convert X-ray energy

into voltage signals, this information is sent to a pulse processor, which measures the signals and passes them onto the analyzer for data display and analysis.

2.3.5 Fourier Transform Infrared Spectroscopy (FTIR)

FTIR is the useful technique to identify the types of chemical bonds. It can be utilized to quantify some of the unknown components in a mixture [13]. FTIR is like molecular fingerprint.

A schematic diagram is shown in figure 2.5 [14]. The beam emitted from the source is passing through an aperture and control the amount of energy on the sample. The beam then enters the interferometer, which produces a signal that has spectral encoding into it. The beam is split into 2 by the beam splitter upon entering the interferometer. One beam reflects off a flat mirror which is fixed in place while the other beam reflects off a flat mirror which allows this mirror to move very short distance away from the beamsplitter. These two beams later recombine to form interferogram. The laser beam incident to the interferometer is used for wave calibration, mirror position control and to collect data of the spectrometer. The beam enters the sample the sample where it is transmitted through the sample surface. Then the detector detects the beam for measurement [14]. In this study the Bruker TENSOR 27 Series FTIR spectroscopy shown in figure 2.6 was used.

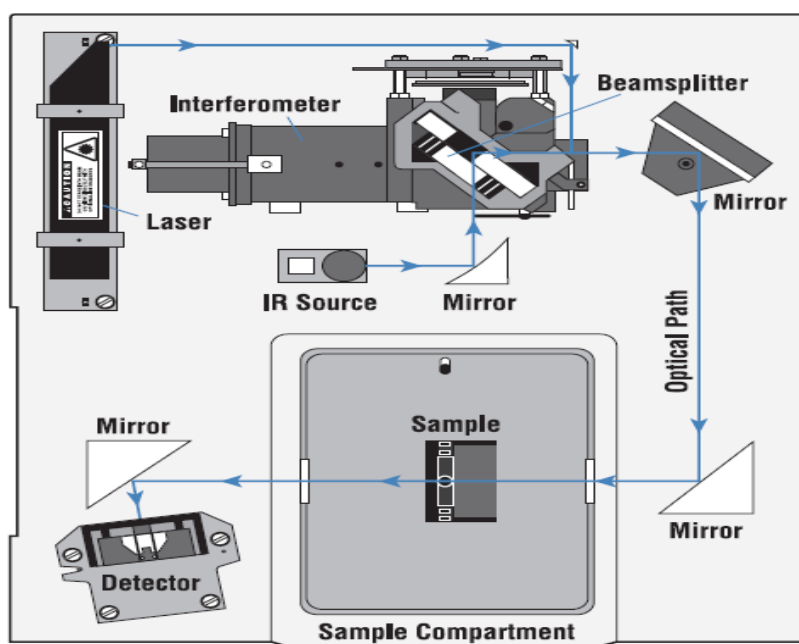


Figure 2.5: A simplified layout FTIR spectrometer [14]



Figure 2.6: Bruker TENSOR 27 Series FTIR spectroscopy

References

- [1] T. A. Singanahally, S. M. Alexander, *Current Opinion in Solid State and Materials Science*, **12**, 44-50. (2008)
- [2] <http://www.igcar.gov.in/benchmark/science/53-sci.pdf> [Accessed 25 November 2011]
- [3] <http://www.dtic.mil/cgi-bin/GetTRDoc?Location=U2&doc=GetTRDoc.pdf&AD=ADA473708>
- [4] K. Kalantar-zader, B. Fry, *Nanotechnology-Enabled Sensors*, ISBN number 978-0-387-68023-1 (Online), Springer US, 2008, p 211-281
- [5] http://serc.carleton.edu/research_education/geochemsheets/techniques/XRD.html [Accessed 30 November 2011]
- [6] M. Razeghi, *Fundamental of solid state engineering*, ISBN number 978-387-28751-5 (online), Springer US, 2006, p521-549
- [7] T. H. Gfroerer, *Encyclopedia of Analytical Chemistry*, R.A. Meyers (Ed.), John Wiley & Sons Ltd, Chichester, 9209, (2000).
- [8] D. B. Bem, PhD Dissertation, University of the Free State (2011)
- [9] http://www.nhml.com/capabilities_Scanning-Electron-Microscopy.cfm [Accessed 19 September 2011]
- [10] <http://www.cranfield.ac.uk/cds/cfi/eds.html> [Accessed 30 November 2011]
- [11] L. D. Hanke, *handbook of analytical methods for materials*, Material Evaluation and Engineering, Inc, (2009)
- [12] <http://www.wcaslab.com/tech/tech2.htm> [Accessed 30 November 2011]
- [13] <http://mmrc.caltech.edu/FTIR/FTIRintro.pdf> [Accessed 16 September 2011]

Chapter III

Synthesis and characterization of $\text{SrAl}_2\text{O}_4:\text{Ce}^{3+}$ using solution combustion method

3.1 Introduction

Phosphorescent phosphors have been widely studied due to their great potential in several applications such as in devices and luminous paints on highways, airports, in textiles materials and as ceramic products [1, 2]. Ce^{3+} ions is one of the most attractive trivalent rare-earth ions with a broad band emission consisting two peaks in the long wavelength UV region. This emission is caused by a 5d–4f transition [3, 4]. In many hosts, where luminescence from the Ce^{3+} 5d state is observed, at least one of the Ce^{3+} components of the 5d states lies below the bottom of the conduction band from which emission occurs. Among various host matrix materials, the aluminates based have widely considered due to their superior properties, namely:

- High energy efficiency
- A wide range of excitation wavelength
- High quenching temperature [5]

Strontium aluminate is an efficient host material with a wide band gap which generates a broadband emission upon doping with rare earth ions or transition metal ions [6, 7]. SrAl_2O_4 belongs to the tridymite structure with lattice parameters, space group ($P2_1$) and a framework of AlO_4 tetrahedra.

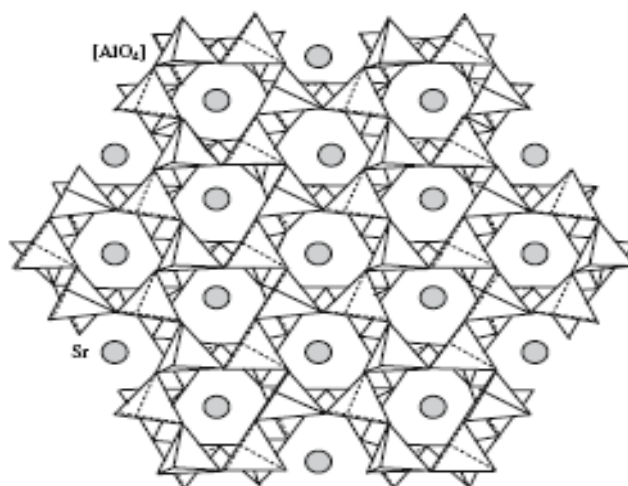


Figure 3.1: Illustration of Monoclinic structure of SrAl_2O_4 ($P2_1$) with the linkage patterns of the $[\text{AlO}_4]$ tetrahedral. The closed gray circles indicate Sr atoms.

Each oxygen ion is shared by two aluminum ions so that each tetrahedron has one net negative charge. The charge balance is achieved by the large divalent cation Sr^{2+} [8, 9]. The synthesis of oxide phosphors has been achieved by many methods like solid state reaction, sol-gel techniques, hydroxide precipitation, microwave heating techniques and combustion method [10]. Aluminates were usually prepared by solid state reaction which requires a long reaction time and a high temperature firing (above $1550\text{ }^\circ\text{C}$) [11, 12]. However, the synthesis temperature can be greatly reduced by using solution combustion method which involves an exothermic reaction between metal nitrates and a fuel (mainly urea) [13]. This synthesis process therefore is very facile, fast (synthesis completed in the order of several minutes), safe and required minimum energy [14, 15].

This chapter reports on the use of the solution combustion method to produce strontium aluminate doped with Ce^{3+} . The effect of different concentration of cerium on the structure, morphology and photoluminescence was investigated.

3.2. Experimental

3.2.1 Synthesis of SrAl_2O_4 doped with Ce^{3+}

$\text{SrAl}_2\text{O}_4:\text{Ce}^{3+}$ powders were synthesized by the solution combustion method using $\text{Sr}(\text{NO}_3)_2$, $\text{Al}(\text{NO}_3)_3 \cdot 9\text{H}_2\text{O}$, $\text{Ce}(\text{NO}_3)_3 \cdot 6\text{H}_2\text{O}$ and $\text{CO}(\text{NH}_2)_2$ as a starting material. Appropriate amounts of starting materials were dissolved in 5ml of de-ionized water and continuously stirred for 30

minutes to obtain a clear solution. The doping concentrations of the Ce^{3+} ions were 0.25, 0.4, 0.5, 0.7, 1, 1.5, and 2 mol%, respectively. The mixed solution was placed into a muffle furnace maintained at 500 °C. In about five minutes the solution boiled and underwent dehydration followed by decomposition with escaping large amount of gases (oxides of nitrogen and ammonia) then spontaneous combustion with enormous swelling produced a foamy and voluminous powder. As soon as the reaction was over, the product was cooled to room temperature. The foamy powders were crushed into powders and the obtained white powders were ready for characterization. A flow diagram describing the preparation of $\text{SrAl}_2\text{O}_4:\text{Ce}^{3+}$ is shown in figure 3.2.

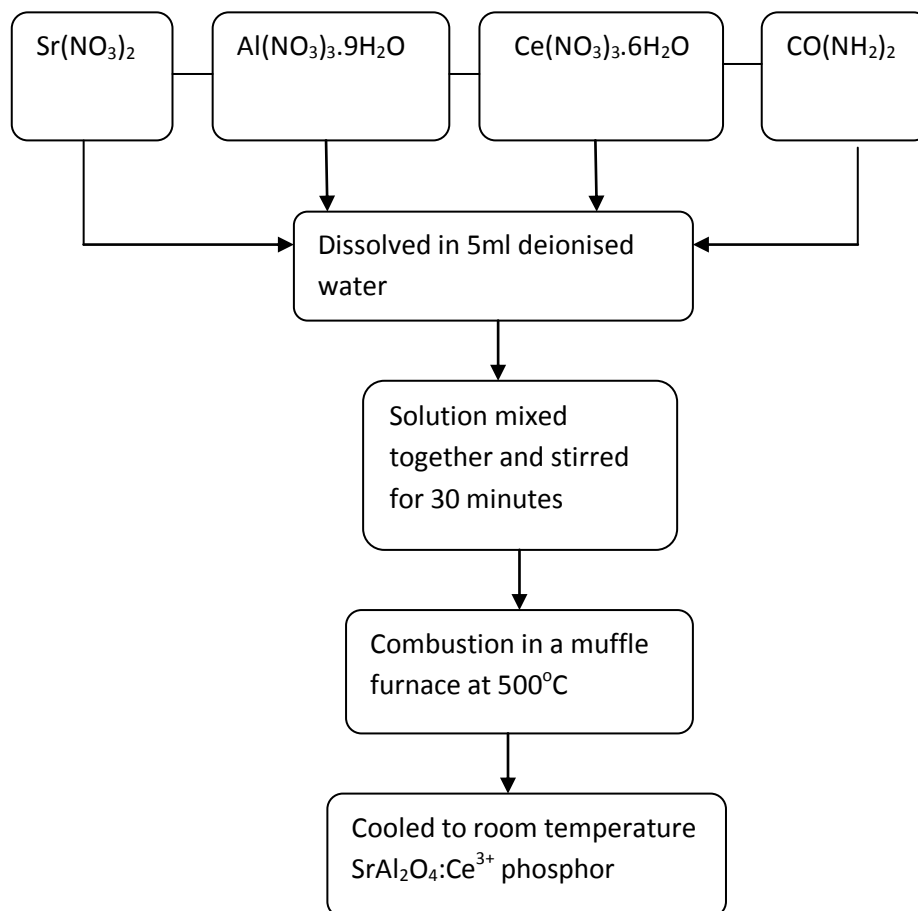


Figure 3.2: Flow diagram depicting the synthesis of $\text{SrAl}_2\text{O}_4:\text{Ce}^{3+}$ phosphor using solution combustion method

3.2.2 Characterization

Crystalline structure and particle size of the phosphor and types of chemical bonds were investigated using D8 advanced AXS GmbH X-ray diffractometer (XRD) and Bruker TENSOR 27 Series FTIR spectroscopy, particle morphology and elemental composition using a scanning electron microscope (SEM) Shimadzu Superscan SSX-550 SEM coupled with an energy dispersive X-ray spectrometer (EDS). PL measurements were made on a Carry Eclipse photoluminescence spectrophotometer system, equipped with a 150 W xenon lamp as the excitation source

3.3 Results and Discussion

3.3.1 X-ray diffraction

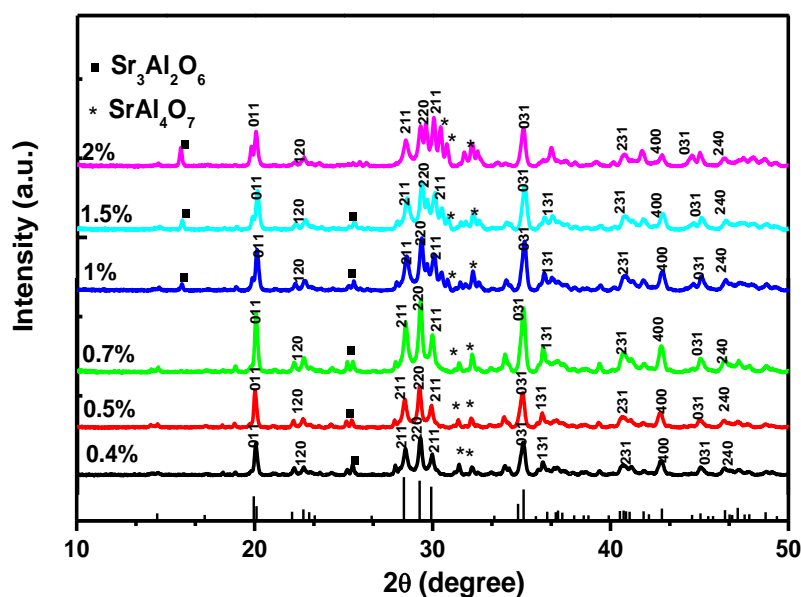
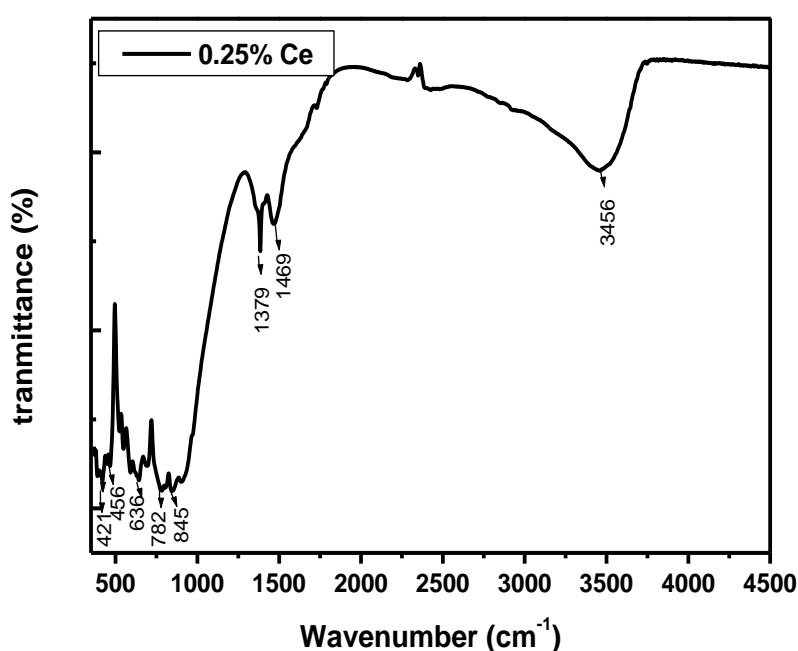


Figure 3.3: XRD patterns of SrAl₂O₄ doped with different concentration of Ce³⁺

Figure 3.3 shows the XRD (X-ray diffraction) patterns of the SrAl₂O₄ powders prepared by solution combustion method for at Ce³⁺ concentrations of 0.4, 0.5, 0.7, 1, 1.5, and 2 mol%. The XRD patterns shows the main peaks of SrAl₂O₄ belong to the monoclinic phase according to the JCPDS file (34-0379). The XRD also indicates some peaks which related to other impurities phases such as Sr₃Al₂O₆ and Sr₃Al₄O₇ that formed during the combustion process. The average particle sizes of the phosphor were estimated using the Scherrer's equation and were shown in table 1.

Table 1: The estimated average particle sizes of SrAl₂O₄ doped Ce³⁺

Peak	2Theta (degree)	FHWM (β)	Particle size (nm)
011	20.041	0.14893	54
211	28.460	0.17833	46
220	29.296	0.16085	51
211	29.950	0.16504	50
031	35.072	0.25094	33
Average =			47

**Figure 3.4: FTIR spectrum of SrAl₂O₄:0.25%Ce³⁺**

3.3.2 FTIR

The FTIR spectrum of the SrAl₂O₄:0.25%Ce³⁺ was shown in Figure 3.4. All the identified bands have been marked in the figure. The bands between 350 and 1000 cm⁻¹ can all be assigned to the IR active vibration modes of SrAl₂O₄. The symmetric bonding of O–Al–O appears at 456 and 421 cm⁻¹. The antisymmetric stretching bands ranging of 588–636 cm⁻¹ are attributed to the Sr–O vibrations. The band located at 845 cm⁻¹ is Sr–O. The bands positioned at 782 and 900 cm⁻¹ originate from the aluminates groups (AlO₄). The two bands at 1379 and 1469 cm⁻¹ are attributed to the C–O vibrations. The band located at 3456 cm⁻¹ is the symmetric vibration of –OH groups [6].

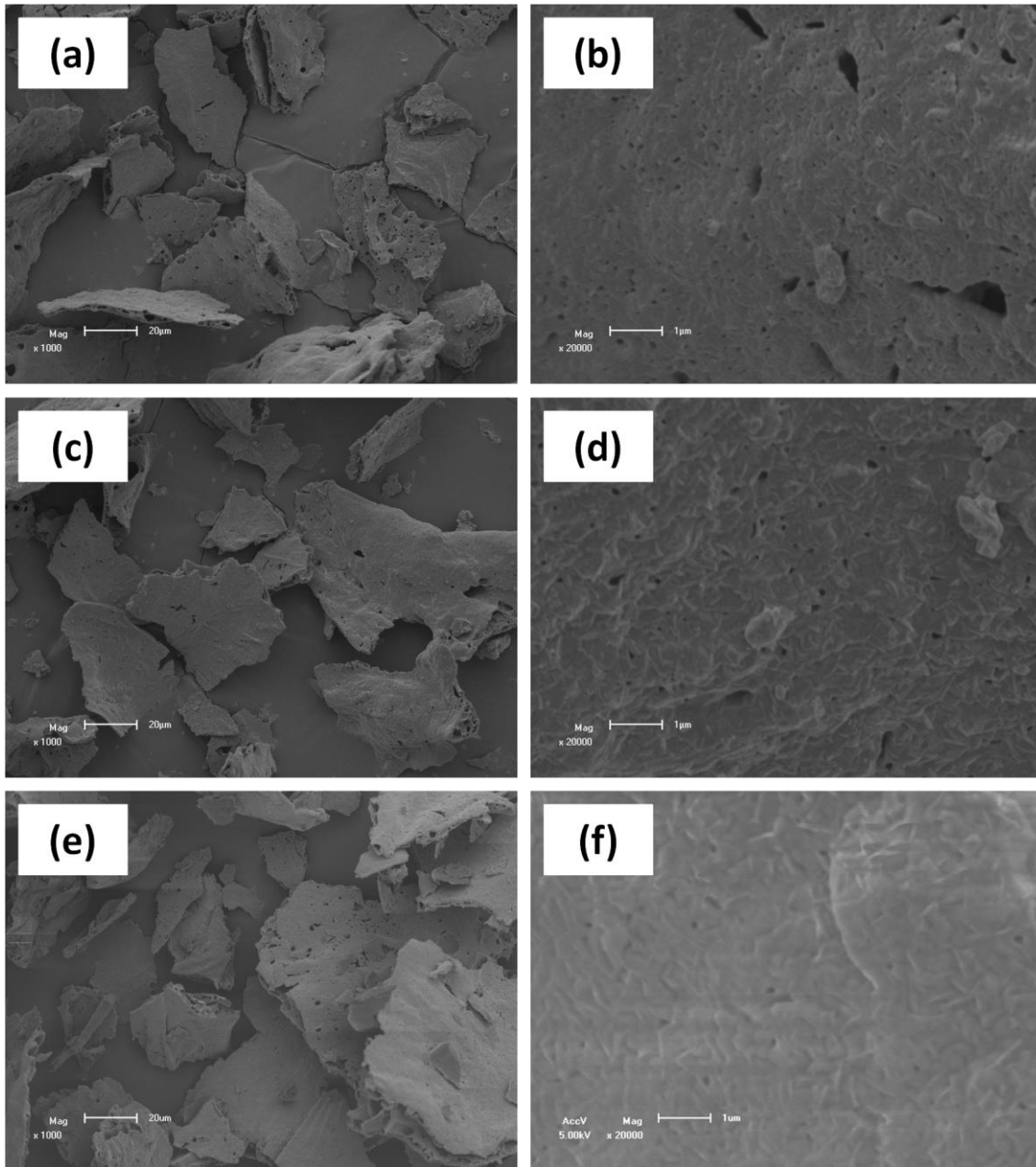


Figure 3.5: SEM images of $\text{SrAl}_2\text{O}_4: 0.25\%\text{Ce}^{3+}$ (a) 1000x magnification (b) at magnification of 20000x. $\text{SrAl}_2\text{O}_4: 1.5\%\text{Ce}^{3+}$ (c) at magnification of 1000x (d) at 20000x magnification. and $\text{SrAl}_2\text{O}_4: 2\%\text{Ce}^{3+}$ (e) 1000x magnification and (f) 20000x magnification

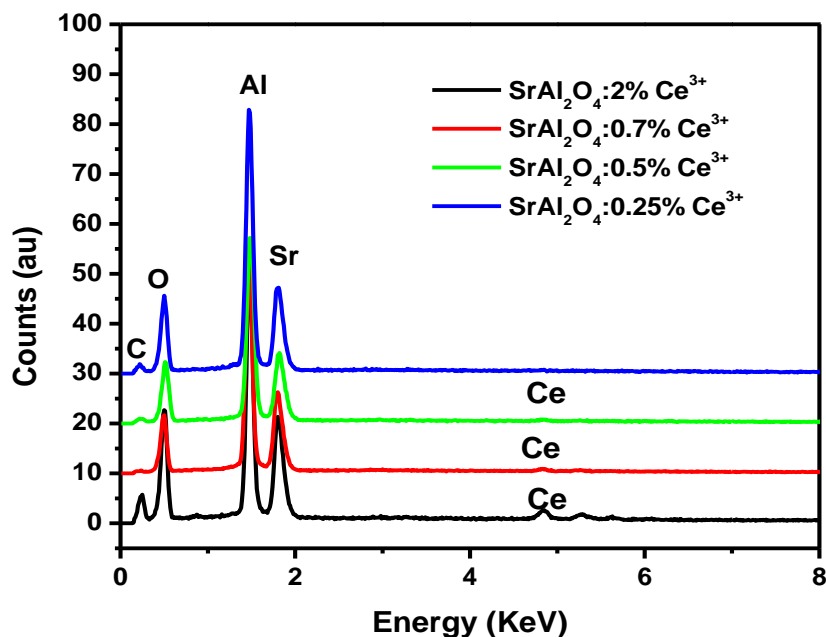


Figure 3.6: EDS spectra of SrAl₂O₄:Ce³⁺

3.3.3 Morphology and EDS compositional analysis

Measurements using scanning electron microscopy (SEM) were carried out to determine the morphology of the sample. Figure 3.5 displays SEM images of strontium aluminate prepared by solution combustion method. The morphologies of different concentration were taken at 1000x and 20000x magnification. It can be seen that the particles were agglomerated. At high magnification the image revealed the small elongated–egg-like shapes on the particles. The surfaces of the foams show a lot of voids and pores formed by the escaping gasses during the combustion reaction. Figure 3.6 shows the EDS spectra of the SrAl₂O₄:Ce³⁺ phosphor. The presence of SrAl₂O₄ in the sample is confirmed with the Sr, Al, and O peaks. The C peak is coming from the carbon tape on which the sample was mounted. The Ce small peak is visible in the spectra due to the present of moderate concentration of Ce³⁺ in the 2, 0.7 and 0.5 mol% samples. For 0.25 mol% of Ce³⁺ in the sample the amount of Ce was too small to be detected by EDS.

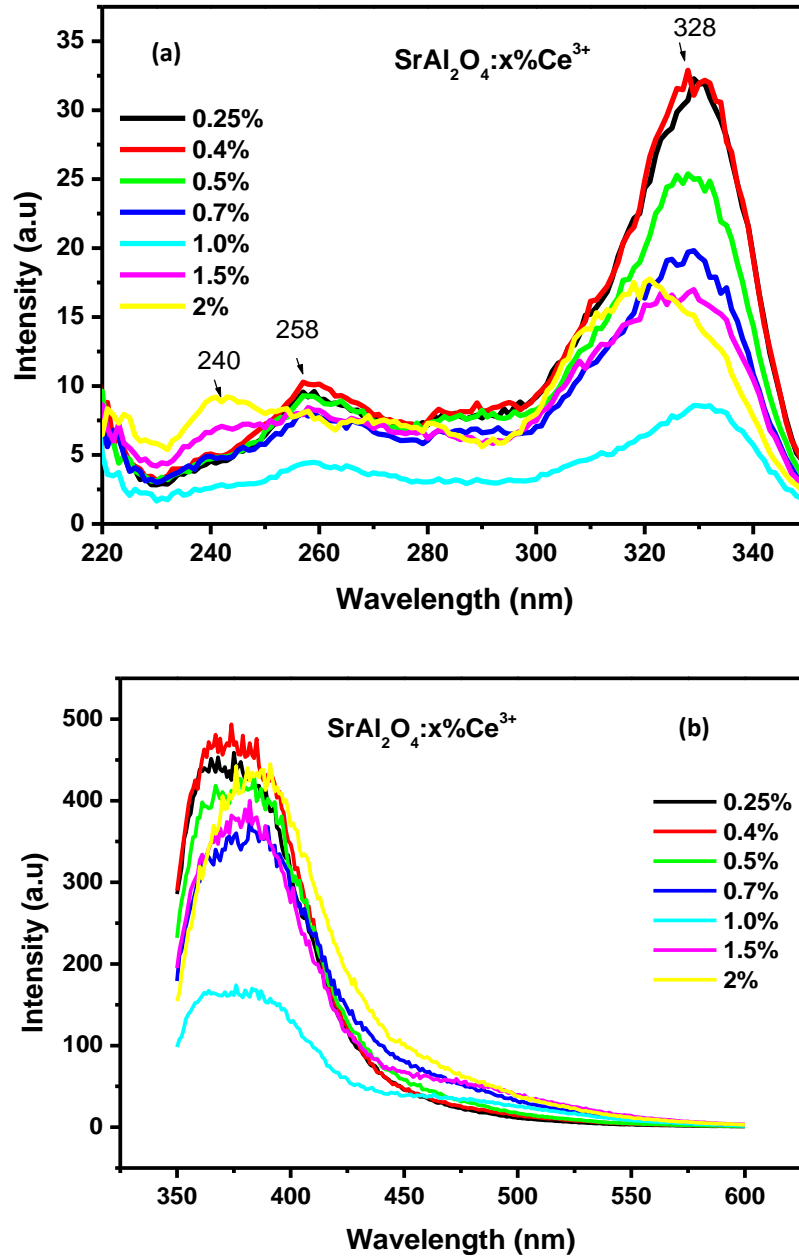


Figure 3.7: Excitation spectra (a) and emission spectra (b) of $\text{SrAl}_2\text{O}_4:x\%\text{Ce}^{3+}$

3.3.4 Photoluminescence spectra

Emission and excitation spectra of Ce^{3+} doped SrAl_2O_4 are shown in Figure 3.7. In figure 3.7(a) the excitation peaks are found at 258 and 328 nm, which correspond to the transitions from the ground state of Ce^{3+} to its crystal field levels of $5D^1$ states. At higher concentrations of 2 and 1.5 mol% Ce^{3+} ion the peaks drift to 240 nm. It can be concluded that at high concentration of cerium the position of the excitation band shifts to a higher energy and this

maybe associate with the crystal field of the Ce^{3+} . The emission bands ranging from 350–425 nm are shown in figure 3.7 (b). Emission of Ce^{3+} usually includes few bands corresponding to the transitions from the lowest 5d excited state to the ${}^2\text{F}_{5/2}$ and ${}^2\text{F}_{7/2}$ states. The observed emission spectra seems to consist of a superposition of peaks at 374 nm and at 384 nm respectively which forms a single broad band. The Ce^{3+} expected emission spectrum is shown in figure 3.7 (c). Figure 3.8 shows the graph of PL maximum intensities of $\text{SrAl}_2\text{O}_4:\text{Ce}^{3+}$ samples as a function of different Ce^{3+} concentrations. The intensity increases at first from 0.25 to 0.4 mol% and then gradually decreases thereafter with the increasing Ce concentration up to 1.0 mol% due to quenching effect. In low Ce concentration ranges, the number of the luminescent centers increases with increasing dopant concentration resulting to a fluorescent enhancement. Further increase in Ce^{3+} concentration leads to a reduction in the distance between the luminescent centers and thereby inducing an energy transfer between the any two luminescent centers. The decreased distance between any two centers results in a decrease of luminescent intensity, a condition known as concentration quenching.

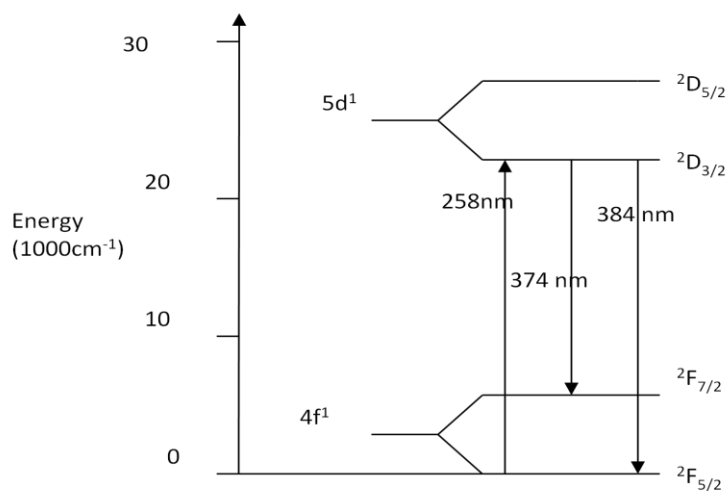


Figure 3.7 (c): Shows Ce^{3+} expected emission spectrum

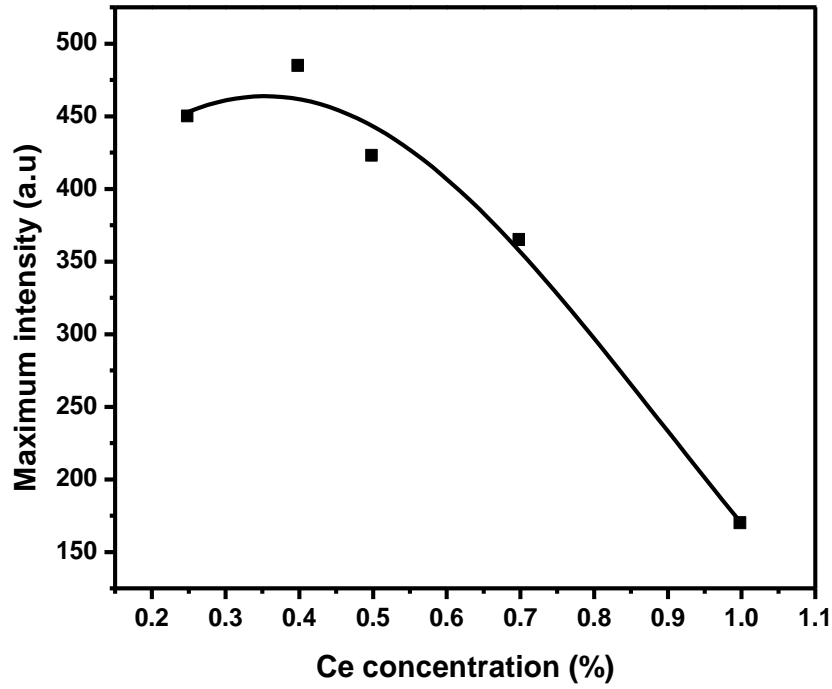


Figure 3.8: Maximum PL intensity as a function of Ce^{3+}

Figure 3.9 shows the decay curves of $\text{SrAl}_2\text{O}_4:\text{Ce}^{3+}$ phosphors with different cerium concentrations. The curves were fitted using the double exponential function.

$$I = A_1 \exp(-t/\tau_1) + A_2 \exp(-t/\tau_2) \quad (3.1)$$

where τ_1 and τ_2 correspond to shorter and longer lifetime constants. A_1 and A_2 are constants and I represent the phosphorescent intensity. The obtained lifetimes are shown in Table 1. It can be seen that the shorter and the longer lifetime decreases with the increases of Ce concentration. The energy transfer between Ce^{3+} ions lead the non-radiative transition rate to increase and concentration quenching, therefore the lifetime becomes shorter.

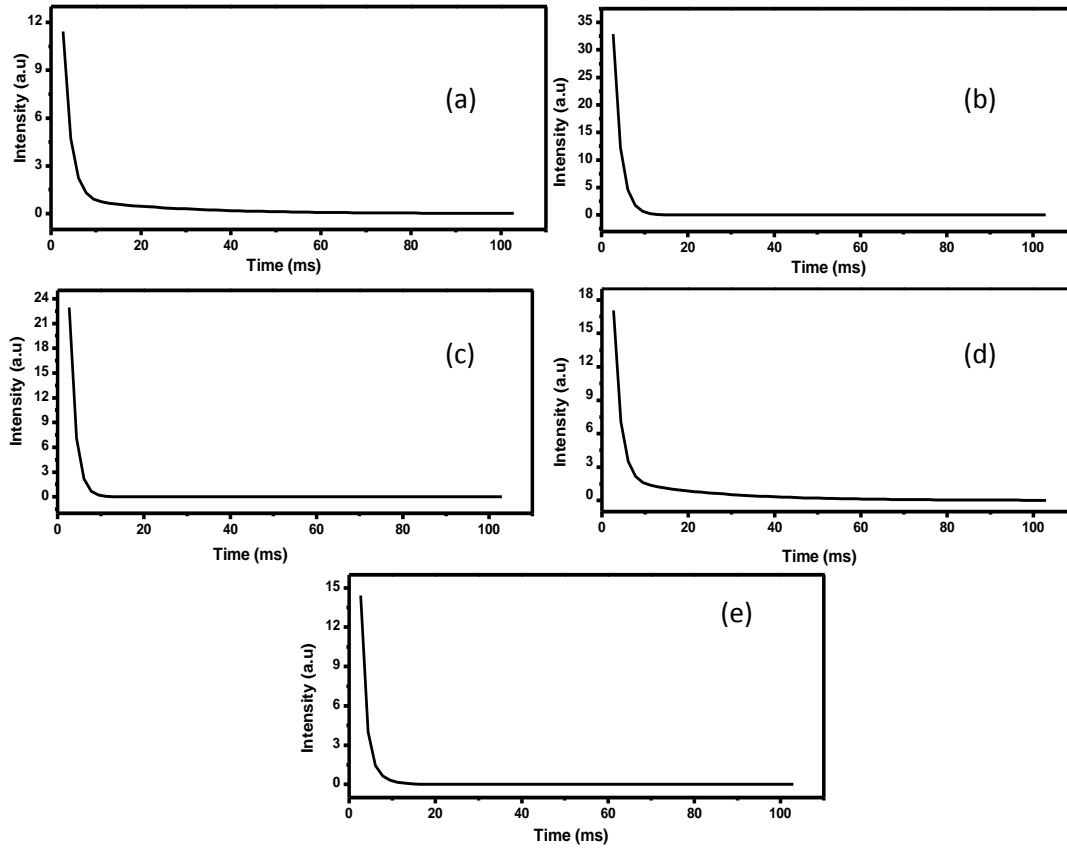


Figure 3.9: Decay curves of SrAl₂O₄:Ce³⁺ phosphor with different Ce concentrations 0.25 mol% (a) 0.4 mol% (b) 0.5 mol% (c) 0.7 mol% (d) and 1.5 mol% (e)

Table 2: Decay parameters of the SrAl₂O₄:Ce³⁺ samples with different doped Ce concentrations

Doping concentration Ce ³⁺ (mol%)	τ_1 (ms)	τ_2 (ms)
0.25	1.6	22.3
0.4	1.7	21.6
0.5	1.3	15.1
0.7	1.1	10.8
1.5	1.2	2.1

3.4 Conclusion

The $\text{SrAl}_2\text{O}_4:\text{Ce}^{3+}$ was successfully synthesized by the solution combustion method using urea as a fuel. The XRD results show that the prepared samples retain the parent SrAl_2O_4 monoclinic crystal structure. FTIR results show all chemical bands for SrAl_2O_4 . SEM morphology revealed the elongated–egg-like shapes on the particles at higher magnifications. Photoluminescence characteristics were investigated and the emission spectra revealed a broad band peak consists of two peaks at 374 nm and 384 nm, which correspond to $^2\text{F}_{5/2}$ and $^2\text{F}_{7/2}$ states. Cerium concentrations have effects on the peak position of excitation spectra. Intensity increased from lower concentration of 0.25 mol% to 0.4 mol% of cerium. At higher concentration of 1 mol% the intensity was decreased due to concentration quenching. The PL of Ce^{3+} exist two decay time constants, including faster and slower rate. The decay time constant of Ce^{3+} first increases with the increase of Ce^{3+} and approaches to the maximum at 0.4 mol% Ce^{3+} , then decreases with the increase of Ce^{3+} .

References

- [1] X. Xuhui, W. Yuhua, Y. Xue, L. Yanqin, Y. Gong, *J. Am. Ceram. Soc.*, **94** [1], 160-163. (2011)
- [2] S. Huajie, C. Donghua, *Luminescence*, **22**, 554-558. (2007)
- [3] F. Zuoling, Z. Shihong, Z. Siyuan, *J. Phys. Chem. B*, **109**, 14396–14400. (2005)
- [4] J. Dongdong, W. Xiao-jun, W. Jia, W. M. Yen, *J. Luminescence*, **122-123**, 311-314. (2007)
- [5] Y. Zhang, L. Li, X. Zhang, D. Wang, S. Zhang, *J. Rare Earth*, **26**, No. 5, p. 656. (2008)
- [6] Z. Ruifang, X. Lin, Q. Weifeng, C. Jiansheng, D. Biao, Z. Ligong, S. Hongwei, *J. Mater Sci*, DOI 10. 1007/s 10853-5723-1
- [7] K.Z. Nadia, B. Igor, K. Andrei, G. Dmitri, M.F.F José, *Nanotechnology*, **21**, 325707 (6pp). (2010)
- [8] H. Ryu, K. S. Bartwal, *Physica B*, **404**, 1714-1718. (2009)
- [9] C. Shin-Hei, K. Nam-Hoon, Y. You-Hoon, C. Sung-Churl, *Journal of Ceramic Processing Research*, **7**, No. 1. 62-65. (2006)
- [10] S. Huajie, C. Donghua, *Luminescence*, **22**, 554-558. (2007)
- [11] L. Zhang, H. Xia, Y. Qiu, D. wang, H. Jiang, *Journal of Rare Earths*, **28**, p. 236. (2010)
- [12] J. M. Rivas-Mercury, A. H. de Aza, P. Pena, *Journal of the European Ceramic Society*, **25**, 3269-3279. (2005)
- [13] Y. Xibin, Z. Chunlei, H. Xianghong, P. Zifei, Y. Shi-ping, *Materials Letters*, **58**, 1087-1091. (2004)
- [14] B. S. Barros, P. S. Melo, R. H. A. Kiminami, A. C. F. M. Costa, G. F. de Sá, Alves Jr S, *J. Mater Sci.*, **41**, 4744-4748. (2006)
- [15] M. S. Nguyen, T. V. Le Thi, K. B. Le Van, N. T. Nguyen, *Journal of Physics, Conference Series*, **187**, (2009) 012017

Synthesis and characterization of green $\text{SrAl}_2\text{O}_4:\text{Tb}^{3+}$ phosphor using solution combustion method.

4.1 Introduction

Long lasting phosphor materials are types of energy storing materials and can light up for a long time in the darkness. The materials can absorb the visible light, store the energy and gradually release the energy as visible light [1]. SrAl_2O_4 is one of the typical matrices for long –duration luminescent materials, which are doped with Eu, Ce, Tb, etc. and is an efficient host lattice with a wide band gap which can generate a broad band emission [2]. As compared with other synthesis methods, the combustion method is very simple, saving energy and it takes only few minutes without requiring subsequent intermediary calcinations stages [3, 4]. Tb^{3+} is one of the most widely used Rare-Earth ions activator for green luminescent materials and has been used widely in tricolor energy saving fluorescent lamp and its emission mainly originate from $^5\text{D}_4$ to $^7\text{F}_j$ ($J=0-6$) transition [5, 6]. The SrAl_2O_4 host belongs to the tridymite-like structure. The structure is formed by three dimensional corner-sharing AlO_4 tetrahedron frame-work. The divalent Sr^{2+} cation balance the charge and occupies an interstitial site within the tetrahedral frame-work [7, 8].

In the present work we have prepared and investigated SrAl_2O_4 phosphor material doped Tb^{3+} ion as an activator. The different concentrations of Tb^{3+} were used and its effect on structure, photoluminescence and luminescence lifetimes was investigated.

4.2 Experimental

The nitrates of Sr, Al, Tb and urea were taken as starting materials, and were dissolved in enough deionized water and kept stirring for 30 minutes until the solution becomes clear. The mixed solution was placed into a muffle furnace maintained at 500 °C. In about five minutes the solution boiled and underwent dehydration followed by decomposition with escaping large amount of gases (oxides of nitrogen and ammonia) then spontaneous combustion with enormous swelling produced foamy and voluminous powder. As soon as the reaction was over, the product was cooled at room temperature. The foamy powder was crushed into powder using pestle mortar and the obtained white powder was characterized.

4.3 Characterization

Crystalline structure and particle size of the phosphor were investigated using the D8 advanced AXS GmbH X-ray diffractometer (XRD), particle morphology and elemental composition using a scanning electron microscope (SEM) Shimadzu Superscan SSX-550 SEM coupled with an energy dispersive X-ray spectrometer (EDS). PL measurements were made on a Carry Eclipse photoluminescence spectrophotometer system, equipped with a 150 W xenon lamp as the excitation source.

4.4 Results and Discussion

4.4.1 X-ray diffraction

Figure 4.1 shows the XRD patterns of $\text{SrAl}_2\text{O}_4:\text{Tb}^{3+}$ phosphor doped with different concentration of Tb^{3+} . It was found that the main peaks formed correspond to the SrAl_2O_4 monoclinic according to the JCPDS, card number (74-0794). Although the main peaks of the crystal structures were observed there were some unknown peaks (marked with stars and dots) and maybe attributed to impurity phases such as $\text{SrAl}_{11}\text{O}_{19}$ and $\text{Sr}_7\text{Al}_2\text{O}_{25}$, or some of the unreacted precursors during the combustion method. The particle sizes of each peak of the phosphor were calculated using the Scherrer's equation and were shown in table 2.

Table 3: Particle sizes for SrAl₂O₄:xTb³⁺ (x=2, 1, 0.5 and 0.4%) phosphor

hkl	020	211	220	211	031	400	
SrAl ₂ O ₄ :xTb ³⁺	Particle sizes						Average
X=2%	88nm	84nm	98nm	94nm	60nm	72nm	82nm
X=1%	94nm	90nm	104nm	108nm	56nm	62nm	86nm
X=0.5%	88nm	88nm	98nm	102nm	56nm	52nm	80nm
X=0.4%	92nm	90nm	98nm	100nm	56nm	52nm	82nm

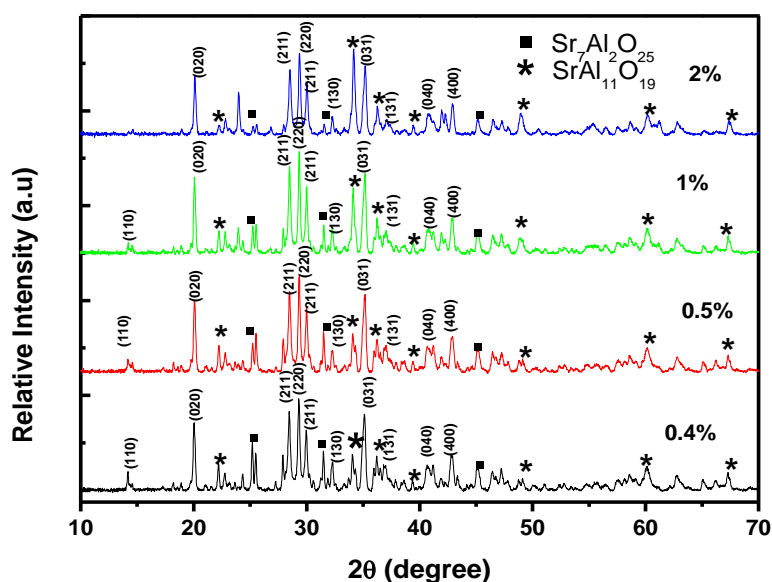


Figure 4.1: XRD patterns of SrAl₂O₄:Tb³⁺ with different concentration of terbium

4.4.2 Morphology

Figure 4.2 Shows SEM morphologies of SrAl₂O₄:Tb³⁺ phosphor prepared by the combustion method that were taken at 1000x magnification. The samples show the pores and voids on the surface that formed by the escaping gases during the combustion method. The morphology of the powders reflects the inherent nature of the combustion process. The images show non uniform and irregular shapes of the particles. All the elements in the SrAl₂O₄:0.5%Tb³⁺ phosphor are observed as shown in the EDS spectrum in figure 4.3. The EDS spectrums are

similar for all samples and therefore the representative spectrum is provided. All the elements included in $\text{SrAl}_2\text{O}_4:\text{Tb}^{3+}$ phosphor were detected in EDS spectra, except for dopant Tb^{3+} , this is because its concentration was too far small to be detected.

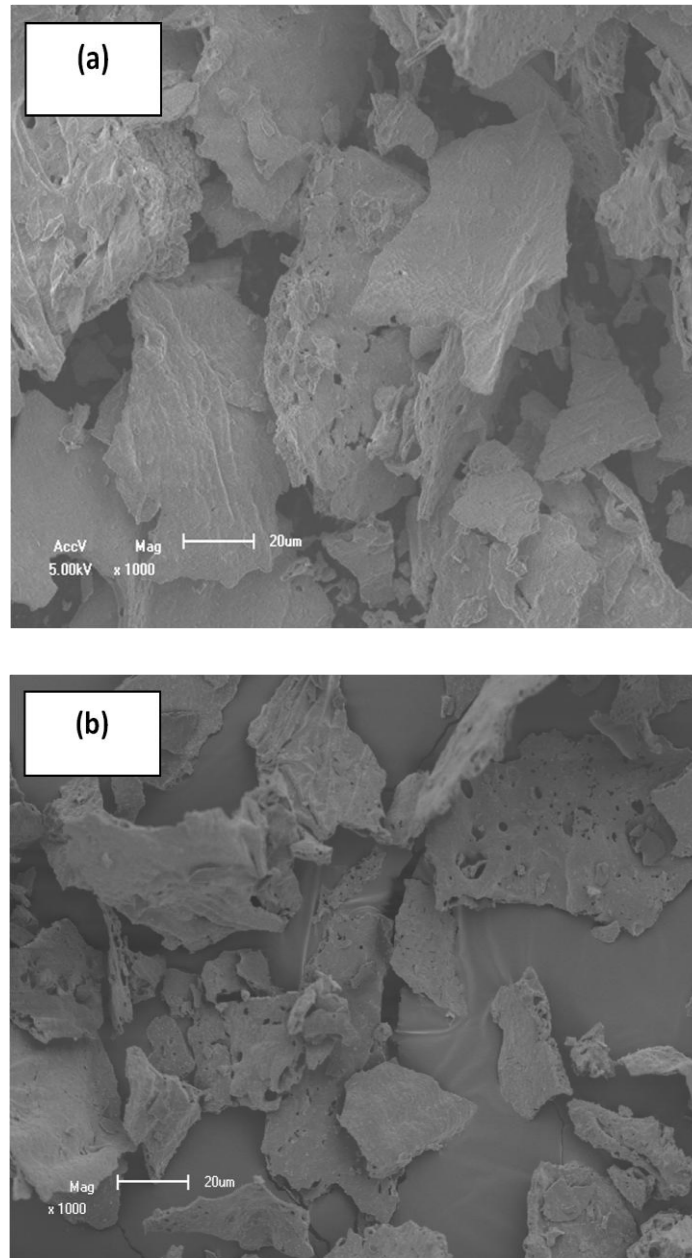


Figure 4.2: SEM image of $\text{SrAl}_2\text{O}_4:0.4\%\text{Tb}^{3+}$ (a) and $\text{SrAl}_2\text{O}_4:0.5\%\text{Tb}^{3+}$ (b) at 1000x magnification.

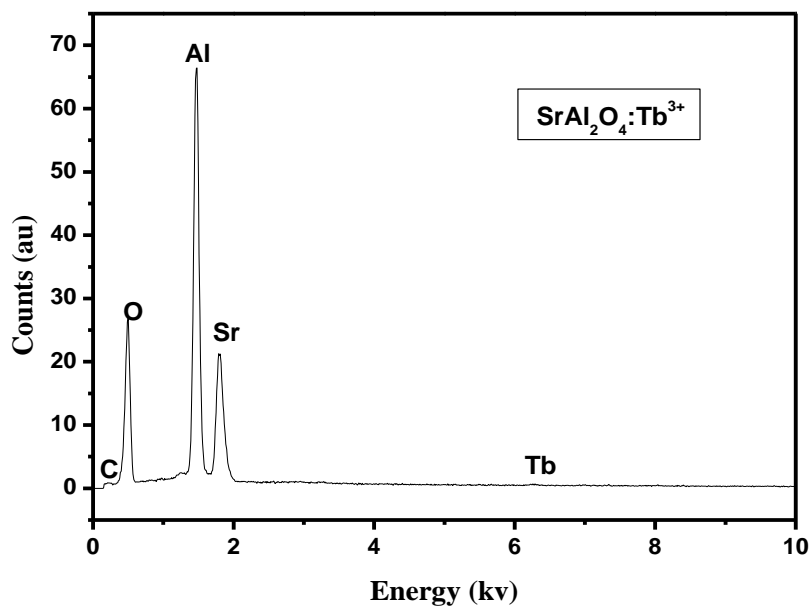


Figure 4.3: EDS spectrum of SrAl₂O₄:0.5%Tb³⁺

4.4.3 Photoluminescence (PL)

Figure 4.4 shows the excitation spectra for the SrAl₂O₄ doped with different moles concentration of Tb³⁺. A broad band centered on 229 nm was observed when 543nm emission of Tb³⁺ was monitored. The strong 229 nm peak is related to the f–d excitation of the Tb³⁺. Figure 4.5 shows the emission spectra of SrAl₂O₄:Tb³⁺ phosphor. The Tb³⁺ doped SrAl₂O₄ phosphor shows a green emission when illuminated by 229 nm. The emission spectra show the weak blue emission in the region of 415–459 nm and strong green emission in 489–622 nm. The 4f–4f emission from ⁵D₄ to ⁷F_J (J= 6, 5, 4, 3) states of Tb³⁺ are found at 489, 543, 585 and 622 nm, respectively. Other emission peaks from the ⁵D₃ to ⁷F_J (J=5, 4, and 3) transitions were also found at 415, 436, and 459nm [8, 9].

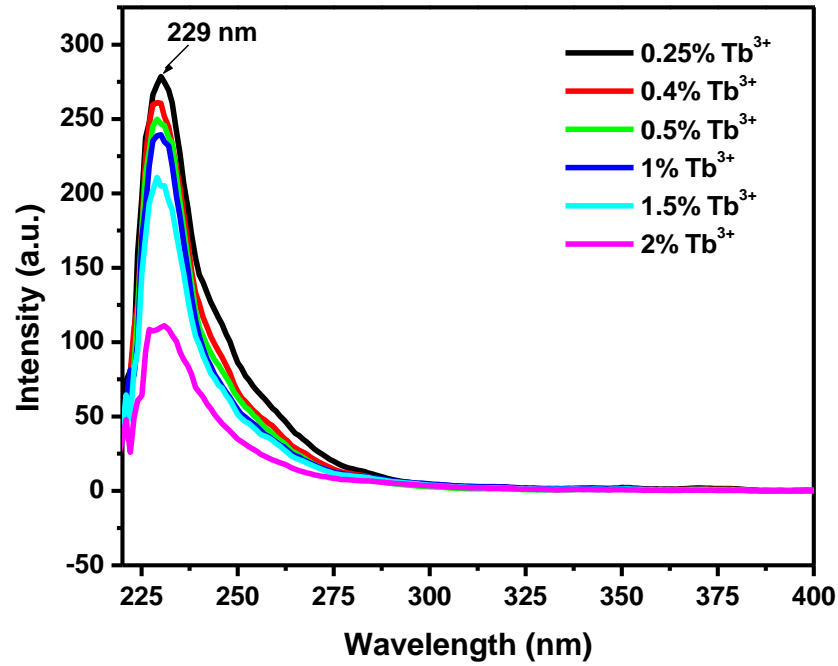


Figure 4.4: Excitation spectra of $\text{SrAl}_2\text{O}_4:\text{Tb}^{3+}$ with different concentration of Tb^{3+} , $\lambda_{\text{em}}=543\text{nm}$

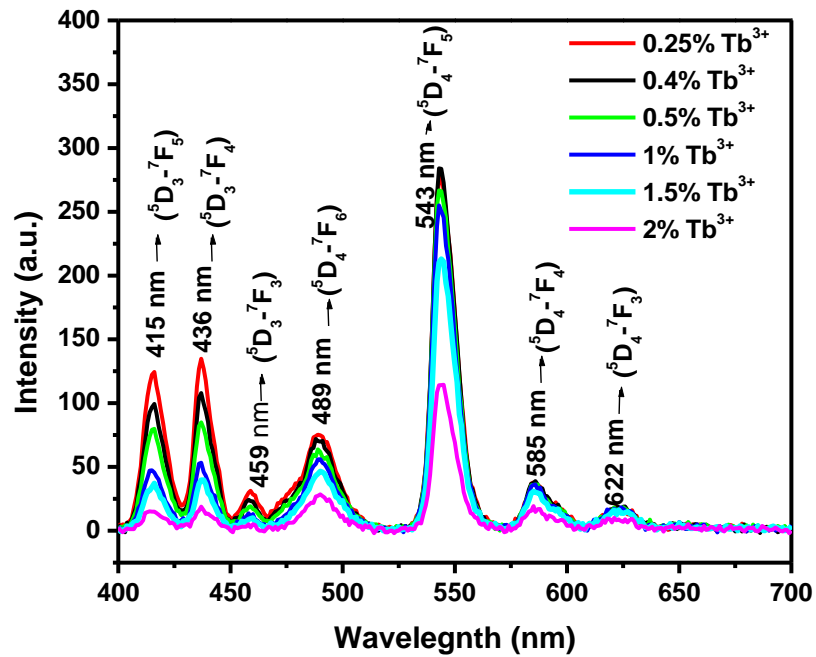


Figure 4.5: Emission spectra of $\text{SrAl}_2\text{O}_4:\text{Tb}^{3+}$ with different concentration of Tb^{3+} , $\lambda_{\text{ex}}=229\text{nm}$

It was found that when the mole concentration of the terbium was increased in the host lattice, there was a significant decrease in intensity of all the terbium transition due to the concentration quenching as shown in figure 4.6. The average distance between luminescent centers is related to the luminescent intensity. The distance between active ions decreases with the increase of doping concentration. When this distance is short enough, the interaction between active ions cause concentration quenching [10].

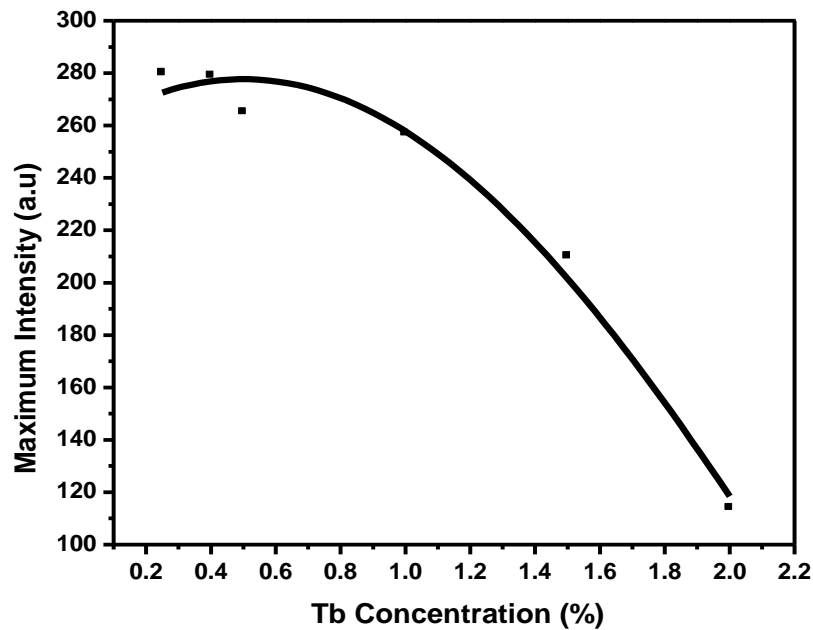


Figure 4.6: Graph of concentration dependence of the emission maximum intensity of Tb^{3+} doped $SrAl_2O_4$

4.4.4 Decay curves and afterglow characteristics

Figure 4.7 shows decay curves of $SrAl_2O_4:Tb^{3+}$ phosphor with different mole concentration of Tb^{3+} . The phosphor showed the rapid decay and long afterglow. The initial intensity of the phosphorescent decreases as the concentration of terbium ions increased in host lattice. As for the mechanism of the long afterglow, it is the reversible energy transfer processes that results in the properties of long afterglow of $SrAl_2O_4:Tb^{3+}$

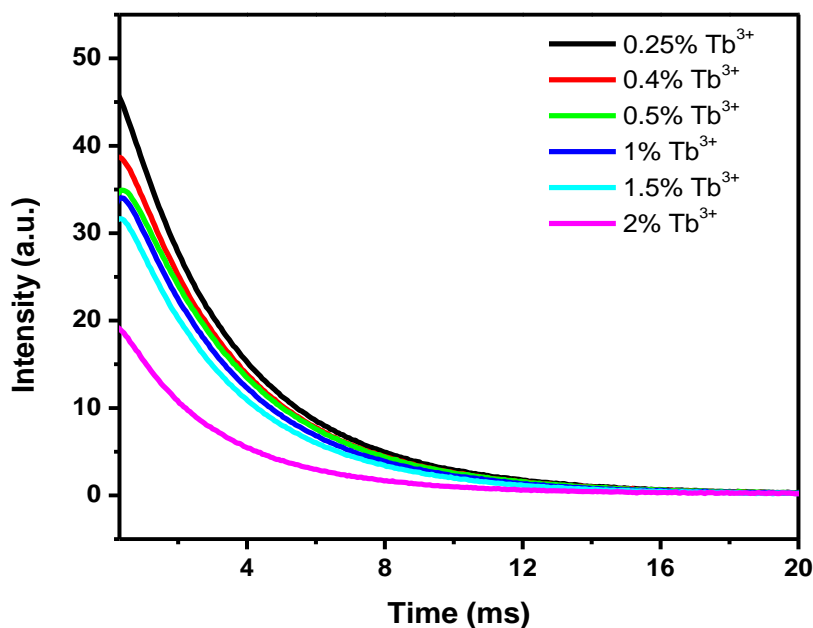


Figure 4.7: Decay curves of $\text{SrAl}_2\text{O}_4:\text{Tb}^{3+}$ of different concentration of Tb.

Tb^{3+} electrons are excited to the excited state and the energy of Tb^{3+} in excited state resonantly transferred to the STE (self-trapped exciton). During the process electrons are excited to the conduction band and produced holes in valence band and the electron in valence band are trapped at electron traps. Electrons in the traps absorbed heat energy and released to conduction band. Then the electrons and the holes in valence band form STE and the energy stored in STE can be transferred to Tb^{3+} to form Tb^{3+} in excited state and Tb^{3+} emits photon and returns to the ground state.

Depicted in figure 4.8 is an illustration of mechanism of $\text{SrAl}_2\text{O}_4:\text{Tb}^{3+}$ phosphor

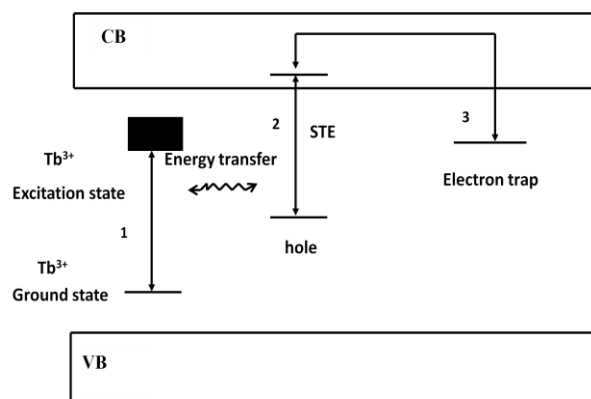


Figure 4.8: Mechanism of $\text{SrAl}_2\text{O}_4:\text{Tb}^{3+}$ phosphor.

The exponential decay times as shown in table 3 are described as (1) initial rapid decay, and (2) slow decay components. The decay constants have higher values for sample with concentration of 0.25 mol% and lower value for sample with 2 mol%.

Table 4: Decay parameters of the SrAl₂O₄:Tb³⁺ phosphor with different Tb³⁺ concentrations

Tb ³⁺ %	0.25%	0.4%	0.5%	1%	1.5%	2%
Compnents	Decay constants					
τ ₁ (ms)	0.25	0.21	0.20	0.17	0.11	0.01
τ ₂ (ms)	3.52	3.42	3.40	3.32	3.39	3.18

4.5 Conclusion

SrAl₂O₄:Tb³⁺ phosphor has been successfully prepared by the combustion method. The XRD results showed that the phosphor has a monoclinic crystal structure. Characteristics green luminescence from Tb³⁺ was observed. The SrAl₂O₄:Tb³⁺ exhibited a predominant green emission at 543 nm, which was assigned to the ⁵D₄ to ⁷F₅ transition of Tb³⁺. The SrAl₂O₄:Tb³⁺ (0.25 mol%) phosphor showed the maximum emission intensity. The non uniform and irregular shapes of the particles was shown by scanning electron microscopy. All the elements of SrAl₂O₄:Tb³⁺ were confirmed by EDS. The decay curves of the phosphors were observed and its intensity was decreased as concentration of Tb³⁺ increased.

References

- [1] H. Song, D. Chen, W. Tang, Y. Peng, *Displays*, **29**, 41-44. (2008)
- [2] F. Zuoling, Z. Shihong, Z. Siyuan, *J. Phys. Chem. B.*, **109**: 14396-14400. (2005)
- [3] S. Huajie, C. Donghua, *Luminescence*; **22**: 554-558. (2007)
- [4] B. S. Barros, P. S. Melo, R. H. G. A. Kiminami, A. C. F. M. Costa, G. A. de Sá, Alves Jr S, *J. Mater Sci*, **41**, 4744-4748. (2006)
- [5] R. K. Verma, K. Kumar, B. B. Rai, *Solid State Science*, **12**, 1146-1151. (2010)
- [6] Y. Zhang, L. Li, X. Zhang, D. Wang, S. Zhang, *J of Rare Earths*, **26**: 656. (2008)
- [7] H. Ryu, K. S. Bartwal, *Physical B*, **404**, 1714-1718. (2009)
- [8] C. Shin-Hei, K. Nam-Hoom, Y. Young-Hoon, C. Sung-Churi, *J of ceramic Processing Research*, **7**: 62-65 (2006)
- [9] C. H. Lu, S. V. Godbole, V. Natarajan, *Materials Chemistry and Physics*, **94**, 73-77. (2005)
- [10] H. Zhu, D. Yang, H. Yang, L. Zhu, D. Li, D. Jin, K. Yao, *J. Nanopart Res*, **10**, 307-312. (2008)

Synthesis and characterization of a green $\text{CaAl}_x\text{O}_y:\text{Tb}^{3+}$ phosphor using solution combustion method

5.1 Introduction

Long lasting phosphor can be used as a type of energy storing material, which can absorb the visible light, store the energy, and then release energy as visible light which lead to a long persistence afterglow in darkness [1, 2]. Afterglow phosphors have attracted considerable attention due to their potential application in various fields, including emergency signs, light sources, luminous paints, optical data storage and dial plates of glow watches, etc. [3, 4]. Among various host matrix materials, aluminates are considered to possess high energy efficiency in a wide excitation wavelength range and a high quenching temperature range [5]. The CaAl_2O_4 host belongs to the stuffed tridymite structure and the framework consists of AlO_4 tetrahedras, with Ca^{2+} ions in the cavities to balance the charge [6]. Terbium is one of the most widely use rare earth ion which emits strongly in the green region. The Tb^{3+} ions luminescence under UV excitation usually consists of four main emission bands around 490, 545, 580 and 620 nm [1]. Compared with other synthesizing methods, like solid state reaction, Sol-gel technique, Microwave heating techniques, etc. the combustion method is very simple, energy saving and takes only a few minutes [7,8] to prepare. The combustion process involves an exothermic reaction with large amount of gas liberation. In this study, we report on the synthesis and characterization of the phosphor calcium aluminate activated with different concentration of Tb^{3+} ions that was prepared with the solution combustion method.

5.2 Experimental procedure

Tb³⁺ doped CaAl_xO_y phosphor was prepared by the solution combustion method. The Ca(NO₃)₂·4H₂O, Al(NO₃)₃·9H₂O, Tb(NO₃)₃·6H₂O, and CO(NH₂)₂ were taken as starting materials and were dissolved in 5ml of deionized water and stirred for 30 minutes. The doping concentrations of the Tb³⁺ ions were 0.25, 0.4, 0.5, 1, 1.5, 2 mol%, respectively. After stirring, the transparent solution was taken into a muffle furnace maintained at a temperature of 500 °C. The solution boiled and underwent dehydration, followed by decomposition with the escape of large amount of gasses (oxides of carbon, nitrogen and ammonia) and then a white foamy and voluminous ash was produced. The whole process was over within less than 5 min, after the product was cooled to room temperature. The foamy powder was crushed into a powder using a pestle mortar and the obtained white powder was characterized. The techniques used for characterization were the D8 advanced AXS GmbH X-ray diffractometer (XRD), Fourier Transform infrared spectroscopy (FTIR Bruker TENSOR 27 Series). Scanning electron microscope (SEM) Shimadzu Superscan SSX-550 SEM coupled with an energy dispersive X-ray spectrometer (EDS), and Photoluminescence (PL) Carry Eclipse photoluminescence spectrophotometer system, equipped with a 150 W xenon lamp as the excitation source.

5.3 Results and Discussion

5.3.1 Structure analysis of CaAl_xO_y:Tb³⁺

Figure 5.1 shows the XRD patterns of phosphors prepared by the solution combustion method. The XRD patterns revealed diffraction peaks of a monoclinic CaAl₂O₄ structure of space group P21/n according to the JCPDS database file number (70-0134). In addition the CaAl₄O₇ phase has been identified as an impurity phase of monoclinic structure. The doping of the different concentration of Tb³⁺ ions on the host did not cause much significant change in the crystal structure of the pristine phase. The FTIR spectra of CaAl_xO_y:xTb³⁺ phosphors were shown in figure 5.2. Absorption bands of the condensed matter AlO₄ located in the range of 900cm⁻¹-700cm⁻¹, isolated AlO₄ located in the range 800 cm⁻¹-650cm⁻¹, however, condensed matter AlO₆ of 500cm⁻¹-680cm⁻¹. Hence these two strong absorptions maybe attributed to AlO₄ liberation at 600cm⁻¹-900cm⁻¹. The absorptions bands at 1500cm⁻¹ and

3450 cm^{-1} are due to vibrations from CO_3^{2-} and OH^- groups, because of CO_2 and H_2O in the air [9, 10].

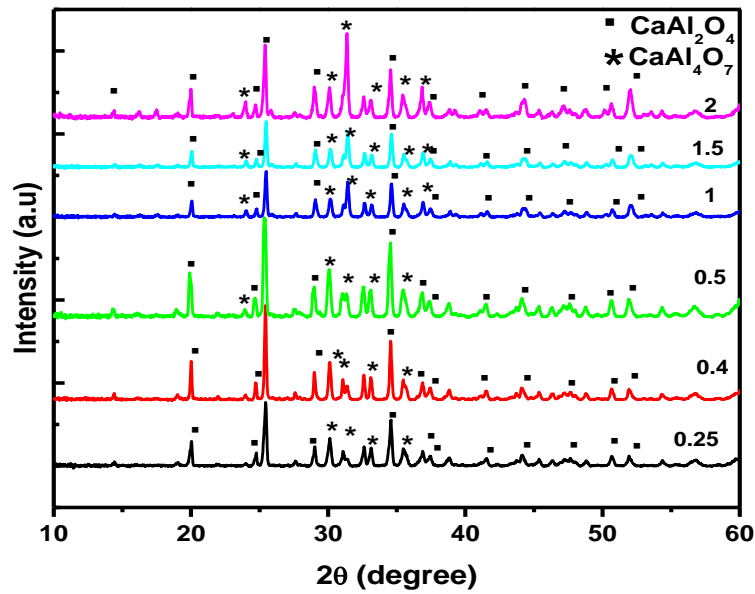


Figure 5.1: X-ray diffraction patterns of CaAl_xO_y with different concentrations of Tb^{3+} ions.

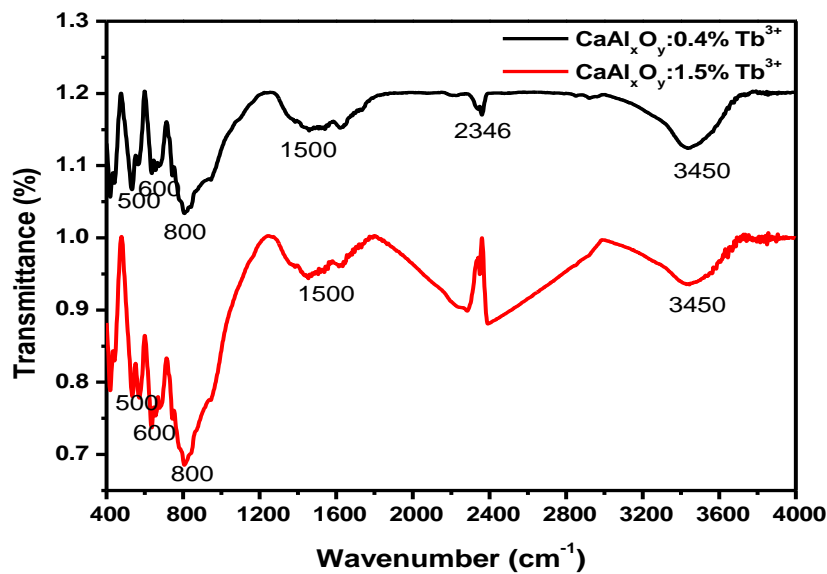


Figure 5.2: FTIR spectra of $\text{CaAl}_x\text{O}_y:\text{Tb}^{3+}$ phosphor (a) 0.4 mol% and (b) 1.5 mol%

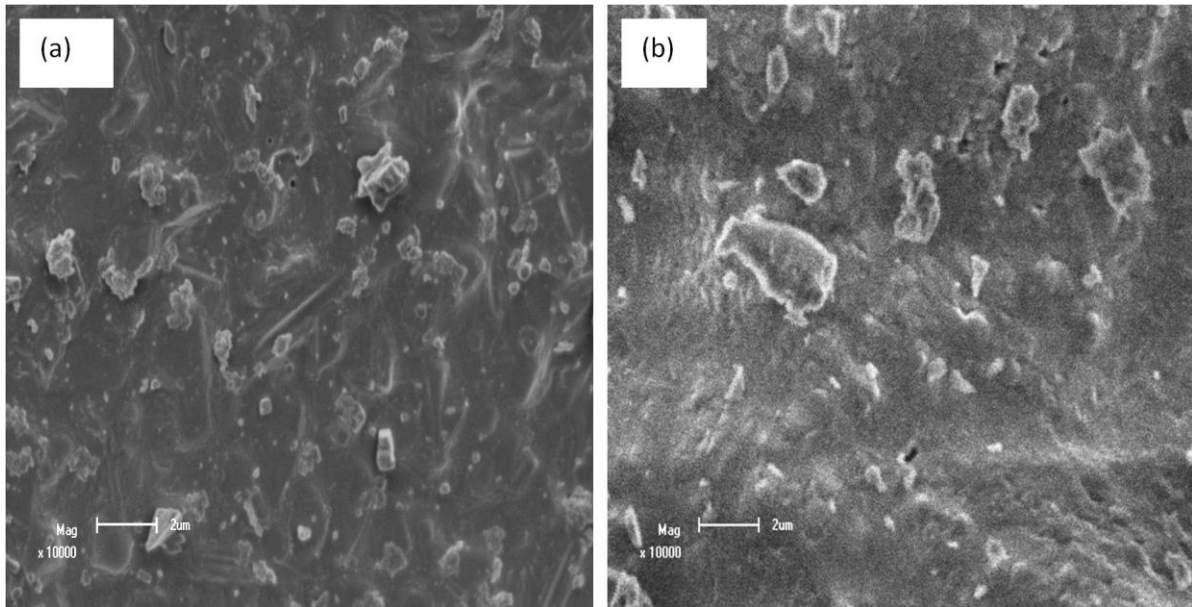


Figure 5.3: SEM image of $\text{CaAl}_x\text{O}_y:\text{Tb}^{3+}$ phosphor (a) 2 mol% and (b) 1.5 mol% at 1000x magnification

5.3.2 Morphology of $\text{CaAl}_x\text{O}_y:\text{Tb}^{3+}$

Figure 5.3 shows the SEM images of $\text{CaAl}_x\text{O}_y:\text{Tb}^{3+}$ of a 2 and 1.5 mol% concentration of Tb^{3+} ions at 1000x magnification, respectively. The surface aspect of the particles is found to be nonspherical and irregular. It was observed that the different concentration of the Tb ions have no effect on the morphology of the samples. Figure 5.4 shows the EDS spectrum of the $\text{CaAl}_x\text{O}_y:\text{Tb}^{3+}$ phosphor. The presence of CaAl_xO_y in the sample is confirmed with the Ca, Al, and O peaks. The C peak is coming from the carbon tape on which the sample was mounted. The Tb small peak is visible in the spectra due to the high concentration of Tb^{3+} in the 2 and 1.5 mol% samples. For 0.5 and 0.25 mol% of Tb^{3+} in the sample the amount of Tb was too small to be detected by EDS.

5.3.3 Photoluminescence properties of $\text{CaAl}_x\text{O}_y:\text{Tb}^{3+}$

Figure 5.5 illustrates the emission spectra of $\text{CaAl}_x\text{O}_y:\text{Tb}^{3+}$ (where $x = 0.25, 0.4, 0.5, 1.0, 1.5$ and 2.0 mol%). The emission spectra show the peaks mainly at 493, 545, 588 and 622 nm respectively when excited with a 239 nm excitation wavelength. The emission peaks are from transition of the $^5\text{D}_4$ state to the $^7\text{F}_J$ ($J = 6, 5, 4, 3$) state. It was found that with an increase in the concentration of Tb in the host lattice there was a significant increase in the intensity of all the peaks.

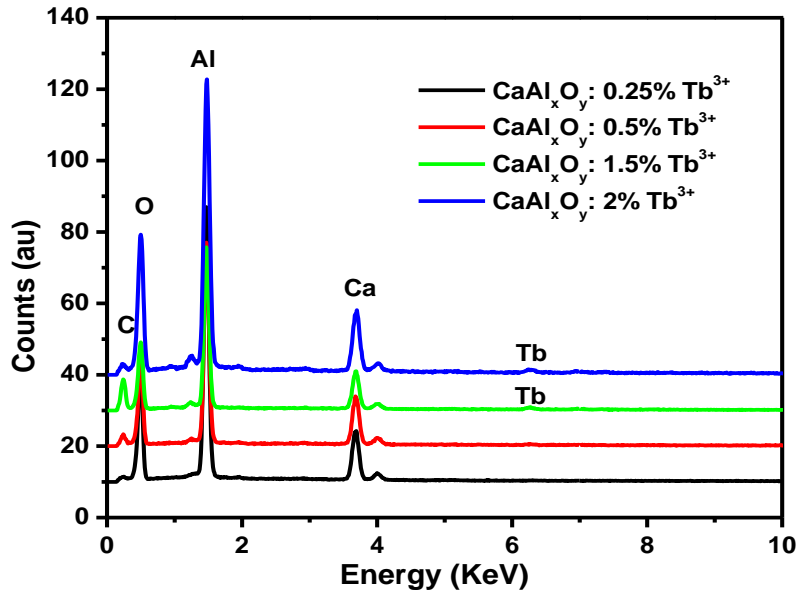
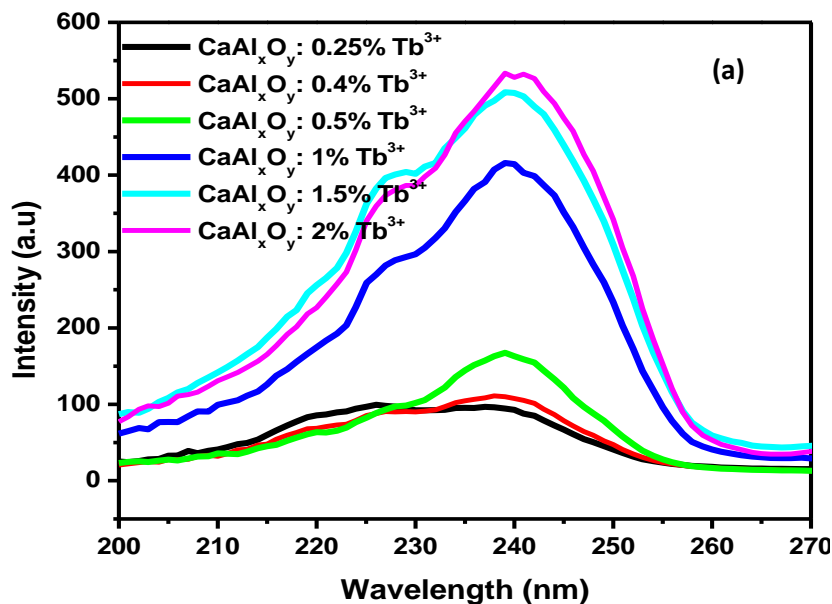


Figure 5.4: EDS spectra of $\text{CaAl}_x\text{O}_y:\text{Tb}^{3+}$ with different concentration of Tb^{3+} ions.

The excitation spectra of the $\text{CaAl}_x\text{O}_y:\text{Tb}^{3+}$ were recorded at an emission of 545 nm. It consists of 4f—5d transitions [2]. The broad band was centered at 239 nm. The intensity increased with an increase in the concentration of Tb^{3+} . The PL intensity of $\text{CaAl}_x\text{O}_y: x\text{Tb}^{3+}$ where x is the different mol percentages of Tb^{3+} ($0.25 \leq x \leq 2.0$) as a function of the Tb^{3+} concentrations is shown in Figure 5.5(c). The emission peaks intensity increased when the amount of Tb increased, and a maximum value was found for $x = 2$ mol%. By increasing Tb^{3+} concentration further, the PL intensity might still increase or quench. In this study we only varied Tb^{3+} concentration up to 2%.



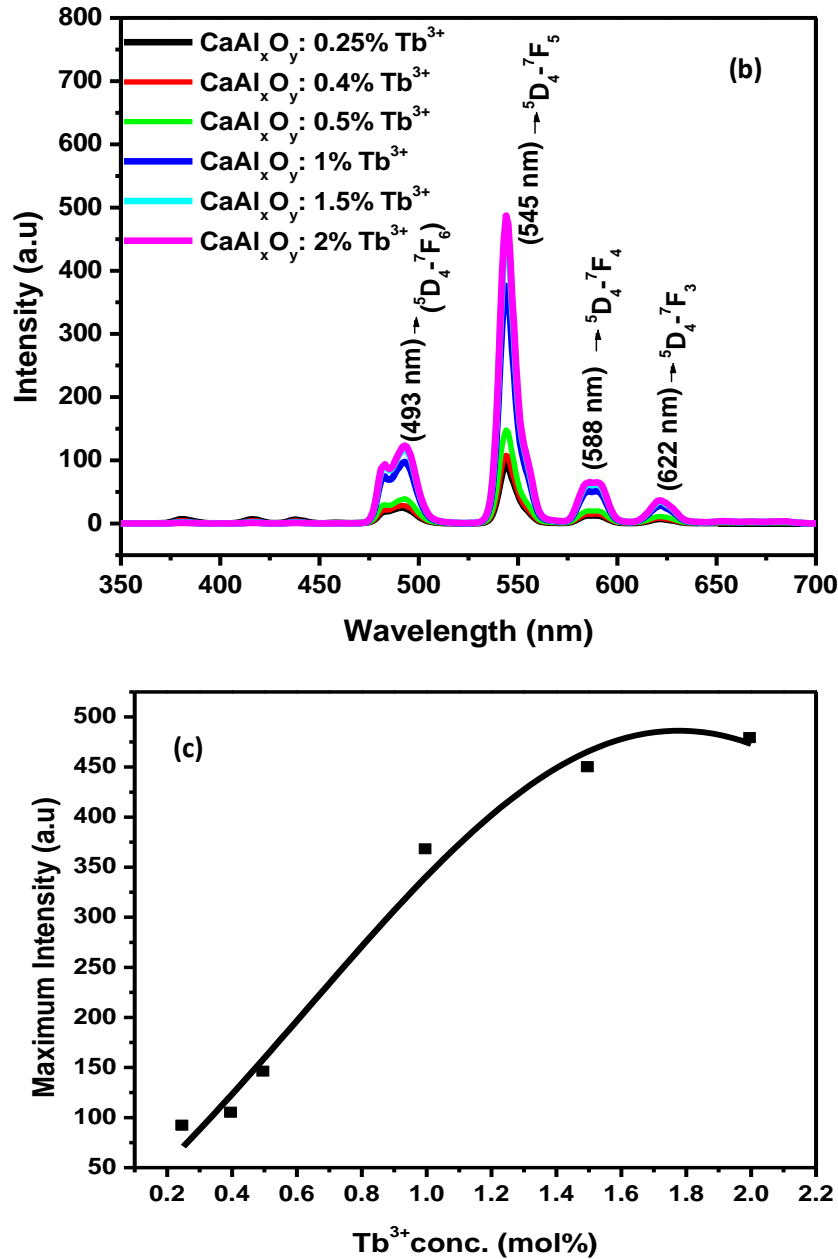


Figure 5.5: (a) Photoluminescence excitation and (b) emission spectra of CaAl_xO_y:Tb³⁺ (c) PL maximum intensity as a function of Tb³⁺ concentration.

Figure 5.6 shows the phosphorescence spectra of the CaAl_xO_y:Tb³⁺ phosphor with a Tb concentration of 0.25, 0.4, 0.5, 1, 1.5 and 2 mol%. The intensity of the phosphorescence decreased quickly at first and then at a slower rate. The decay parameters for the fitting data are listed in table 4. The decay times of sample doped with higher concentration of 2 mol% is longer than that of sample doped with small concentrations. The initial luminescence brightness was improved from 48 a.u to 147 a.u and the long afterglow time was prolonged from 10 ms to 20 ms.

Table 5: Decay parameters of the $\text{SrAl}_x\text{O}_y:\text{Tb}^{3+}$ phosphor with different Tb^{3+} concentrations

Doping concentration Tb^{3+} (mol%)	τ_1 (ms)	τ_2 (ms)
0.25	0.50	1.58
0.4	0.53	1.47
0.5	0.74	1.59
1.0	0.92	1.87
1.5	0.94	1.94
2	1.09	2.04

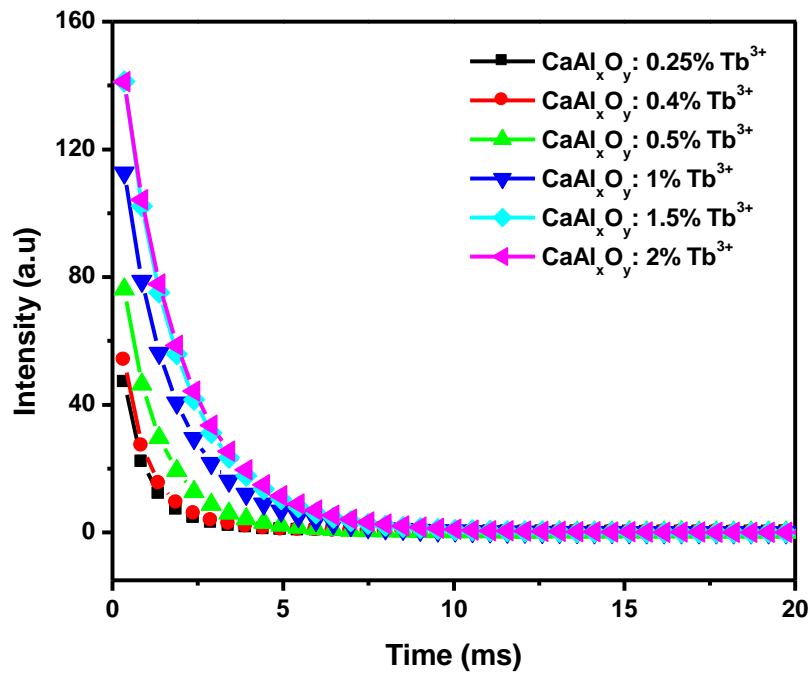


Figure 5.6: Decay curves of $\text{CaAl}_x\text{O}_y:\text{Tb}^{3+}$ phosphor for different Tb^{3+} concentration as indicated.

5.4 Conclusion

$\text{CaAl}_2\text{O}_4:\text{Tb}^{3+}$ phosphor was successfully synthesized by the solution combustion method. The XRD results implied that the phosphor has a monoclinic structure. The increase of the Tb^{3+} concentration in the sample showed a significant enhancement in the emission intensity of the phosphor and the optimum intensity was found at $x=2$ mol%. SEM morphology showed the nonspherical and irregular particles. The brightness and the afterglow properties were enhanced with a higher doping Tb^{3+} concentration of 2 mol%.

Reference

- [1] S. Huajie, C. Donghua, T. Wangjun, P. Yuhua, *Displays*, **29**, 41-44. (2008)
- [2] L. Zhengwei, L. Yingliang, *Materials Chemistry and Physics*, **93**, 129-132. (2005)
- [3] H. SHideo, K. Takeru, K. Hiroshi, Y. Masaaki, Y. Yoshinori, S. Naruhito, *J. Phys. Condens. Matter*, **10**, 9541-9547. (1998)
- [4] X. Xhuhui, W. Yuhua, Y. Xue, L. Yanqin, G. Yu, *J. Am. Ceram. Soc*, **94** [1] 160-163. (2011)
- [5] Y. Zhang, L. Li, X. Zhang, D. Wang, S. Zhang, *Journal of Rare Earths*, **26**, No 5, p.656. (2008)
- [6] C. Shin-Hei, Y. Nam-Hoon, Y. Young-Hoon, C.Sung-Churl, *Journal of Ceramic Processing Research*, **7**, No.1, pp. 62-65. (2006)
- [8] B. S Barrows, P. S melo, R. H. G. A. Kiminami, A. C. F. M. Costa, G.F. de Sá G F, Alves Jr S, *J Mater Sci.*, **41**, 4744-4748. (2006)
- [9] C. B. Fu, H. J. Dong, C. Y. Lui, Y. P. Wang, *Optoelectronics and Advanced Materials-Rapid Communications*, **4**, No. 1, p. 73-76. (2010)
- [10] X. Y. Zhang, H. J. Dong, Z. M. Mei, *Optoelectronics and Advanced Materials-Rapid Communications*, **4**, No. 1, p. 28-32. (2010)

Chapter VI

Preparation and characteristics of $\text{Y}_3\text{Al}_5\text{O}_{12}:\text{Eu}^{3+}$ phosphor by solution- combustion method

6.1 Introduction

Yttrium aluminum garnet, with a chemical formula of $\text{Y}_3\text{Al}_5\text{O}_{12}$ (YAG) has wide application from conventional structure ceramics to photonics due to its high resistance to irradiation damage [1, 2]. The rare-earth doped YAG powders are also widely used as phosphors in cathode-ray tubes, plasma display panels (PDP), field emission, vacuum fluorescent displays (VFD) and electroluminescent [3, 4]. YAG is a well known inorganic compound with good physical and optical properties, and is often used as the host material of full color phosphors by doping it with material such as europium (Eu), terbium (Tb), cerium (Ce), dysprosium (Dy), and thulium (Tm) [5]. YAG:Eu phosphor powder can be synthesized by many methods such as solid-state method, hydroxide co-precipitation, combustion synthesis, pyrolysis of metal nitrate or sulfate mixtures, sol- gel, etc [6]. These methods proved effective in lowering YAG formation temperature and in improving the phase purity of the final product. The solid state method is more feasible than others in terms of operation and a large scale production, but it requires a long reaction time 2 to 6 hours and calcinations at high temperature (2000-2200 °C) [7,8]. The phosphor powder prepared by chemical methods has general advantages such as high purity, better homogeneity and finer grain size. Some preparation processes are complicated and also require long processing time. The combustion method is attractive because of low synthesis temperature and is very simple, safe, and energy saving [9-11]. In this study, we used the solution combustion method to produce $\text{Y}_3\text{Al}_5\text{O}_{12}:\text{Eu}^{3+}$ phosphor

powder. The effect of Eu concentration on structure morphology and luminescence properties was investigated.

6.2 Experimental Procedure

Eu³⁺ doped Y₃Al₅O₁₂ phosphor was prepared by the solution combustion method. The (Y(NO₃)₃.6H₂O, Al(NO₃)₃.9H₂O, (Eu(NO₃)₃.6H₂O and CO(NH₂)₂) were taken as starting materials and were dissolved in 10ml of deionized water and stirred for 30 minutes. The doping concentrations of the Eu³⁺ ions were 0.2, 0.4, 0.7, 1.4 mol%, respectively. After stirring, the transparent solution was taken into a muffle furnace maintained at a temperature of 500 °C. The solution boiled and underwent dehydration, followed by decomposition with the escape of large amount of gasses (oxides of carbon, nitrogen and ammonia) and then a white foamy and voluminous ash was produced. The whole process was over within less than 5 min, after the product was cooled to room temperature. The foamy powder was crushed into a powder using a pestle mortar and the obtained white powder was used for characterization. The techniques used for characterization were X-ray diffraction (XRD, D8 advanced AXS GmbH) to identify the crystalline properties of the particles, Scanning electron microscope (SEM, Shimadzu Superscan SSX-550) used to analyze the size and morphology of the particles, PL (Cary Eclipse Photoluminescence Spectrophotometer equipped with a 150 W xenon lamp) was used to measure the excitation spectra and emission spectra.

Energy dispersive X-ray spectrometer (EDS) was used to identify the elemental composition and Fourier Transform infrared spectroscopy (FTIR Bruker TENSOR 27 Series) to identify the types of chemical bonds.

6.3 Results and discussion

6.3.1 X-ray diffraction and morphology

Figure 6.1 shows the X-ray spectra of the Y₃Al₅O₁₂:Eu³⁺ phosphors with different concentration of Eu. No diffraction peaks appear for the phosphor doped with 1.4% Eu. The main diffraction peaks of the phosphors can be indexed as Y₃Al₅O₁₂ tetragonal phase according to the JCPDS file (09-0310). Some impurities are detected during the combustion method and are attributed to other phases such as Al₂Y₄O₉ and YAlO₃. The scanning electron micrographs of Y₃Al₅O₁₂:Eu³⁺ phosphor taken at 1000x with 0.4, 0.7 and 1.4 mol% are

shown in Figure 6.2. The image of $Y_3Al_5O_{12}$ reveals the formation of agglomerate structure. The SEM images show the several small particles around the pores. This is the result of escaping of gas with high pressure and the pores are formed with the formation of small particles near the pores [12]. Figure 6.3 shows the FTIR spectra of the $Y_3Al_5O_{12}:Eu^{3+}$ phosphors. All the common bands in both spectrums exist such as the O-H band at 3439 cm^{-1} , 3481 cm^{-1} , H_2O vibration band at 1648 cm^{-1} , and 1635 cm^{-1} . The bands at 1384 cm^{-1} and 1356 cm^{-1} are related to NO_3^- groups. Bands at 2370 cm^{-1} and 2397 cm^{-1} appear which originate from the trace CO_2 trapped in combustion products. Peaks observed in the 300 cm^{-1} – 1000 cm^{-1} region are due to metal-oxygen stretching and bending vibrations. The band at 662 cm^{-1} which appears in 0.7% Eu is characteristic of Al–O vibrations, and bands at 439 cm^{-1} and 398 cm^{-1} in both concentrations are characteristic of Y–O vibrations. The metal-oxygen absorption bands indicate that YAG phase has formed [12, 13]. All elements in the $Y_3Al_5O_{12}:Eu^{3+}$ phosphors are present as shown in figure 6.4. The presence of $Y_3Al_5O_{12}:Eu^{3+}$ in the sample is confirmed with the Y, Al, O, and Eu peaks. The C peak is coming from the carbon tape on which the sample was mounted.

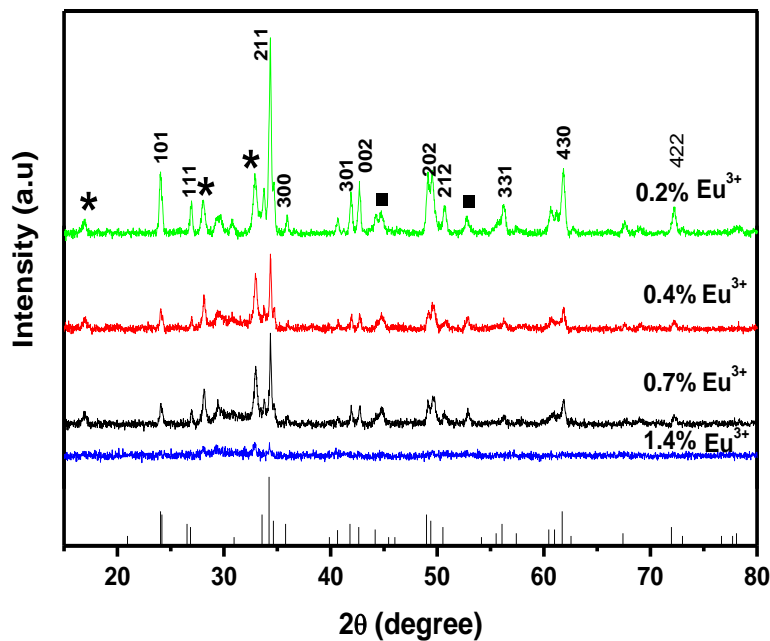


Figure 6.1: XRD pattern of $Y_3Al_5O_{12}:Eu^{3+}$ phosphor

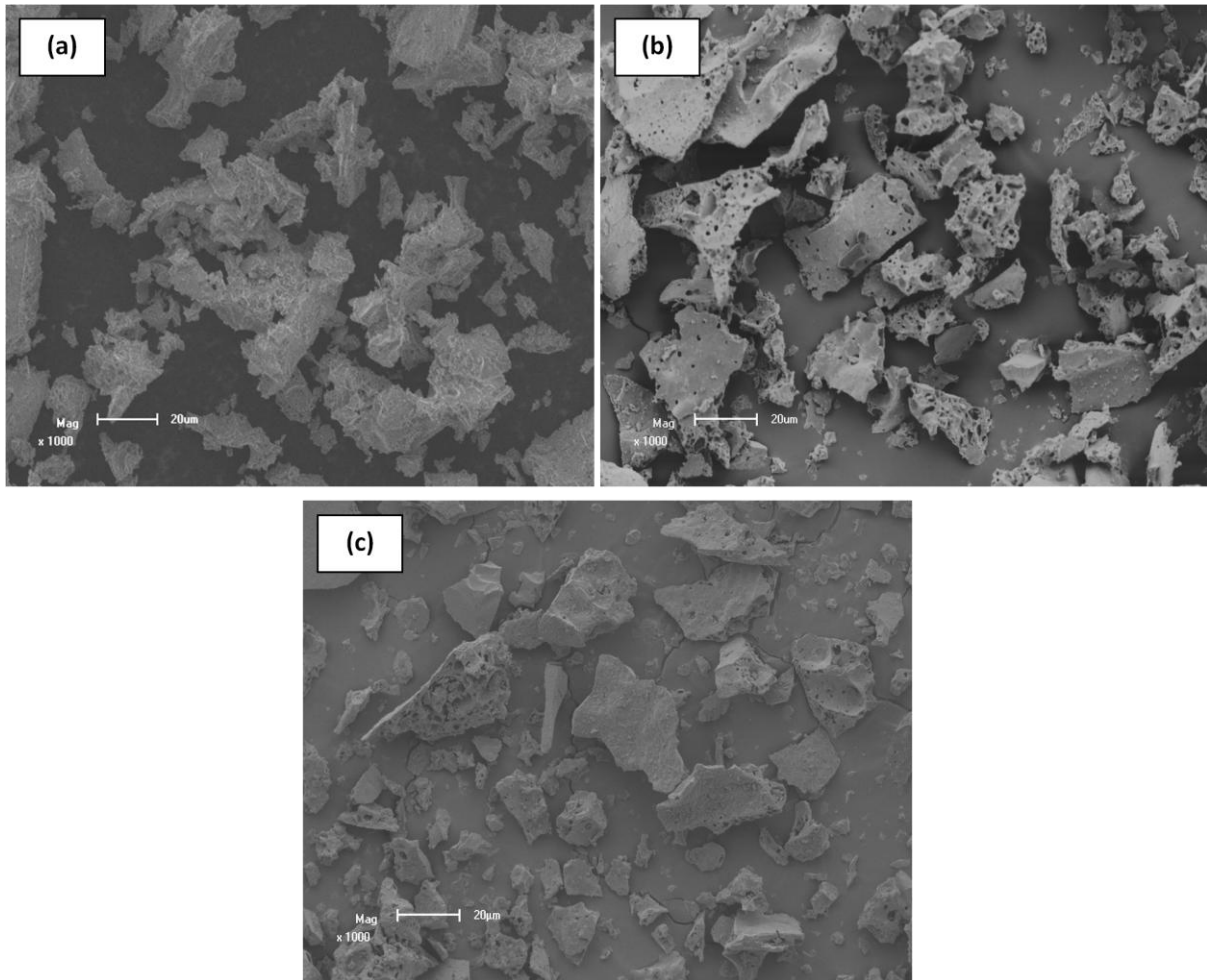


Figure 6.2: SEM photographs of $Y_3Al_5O_{12}:Eu^{3+}$ phosphor doped 0.4 mol% (a) 0.7 mol% (b) and 1.4 mol% (c) of Eu^{3+} respectively.

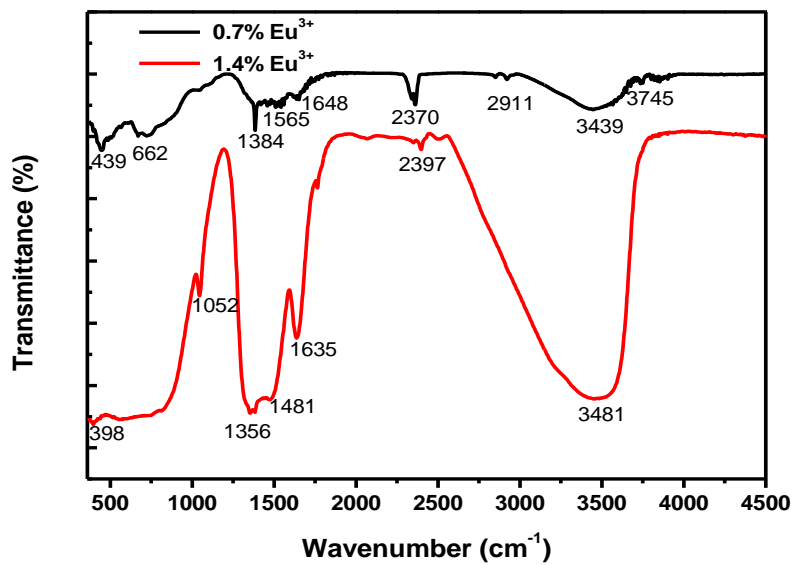


Figure 6.3: FTIR spectra of $Y_3Al_5O_{12}:Eu^{3+}$ phosphor

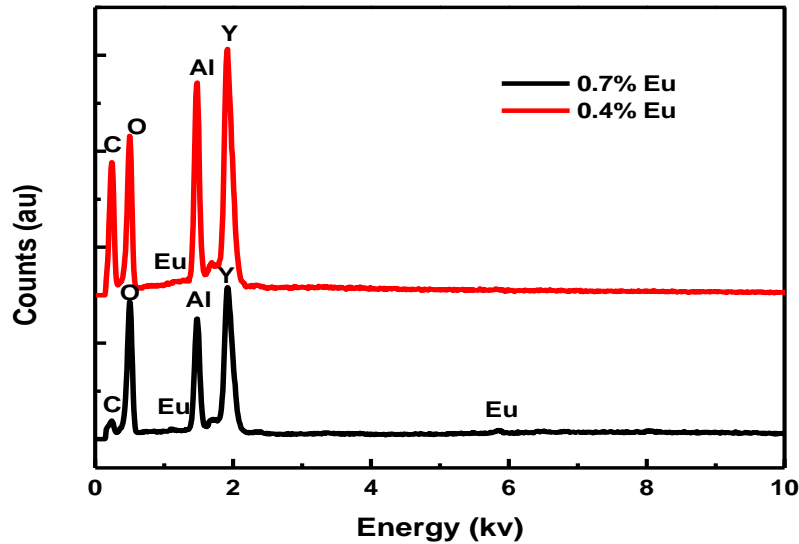


Figure 6.4: EDS Spectra of $\text{Y}_3\text{Al}_5\text{O}_{12}:\text{Eu}^{3+}$

6.3.2 Photoluminescence

Figure 6.5 shows the excitation spectra of $\text{Y}_3\text{Al}_5\text{O}_{12}:\text{Eu}^{3+}$ phosphor containing different concentration of Eu monitored at an emission of 615 nm. The excitation spectra consist of the charge transfer band of $\text{Eu}^{3+}-\text{O}^{2-}$ association in the short ultraviolet region and the bands that are in the longer spectral region are corresponding to the f-f transitions within the $\text{Eu}^{3+} 4f^6$ configuration [3]. The most intense band at 395 nm is associated with the ${}^7\text{F}_0-{}^5\text{L}_6$ transition. Emission spectra of $\text{Y}_3\text{Al}_5\text{O}_{12}:\text{Eu}^{3+}$ phosphor prepared at different concentration of europium are shown in Figure 6.6 as observed in the red spectral area. Three major emission peaks were observed at 592, 615, and 628 nm, corresponding to the ${}^5\text{D}_0 \rightarrow {}^7\text{F}_1$ (592 nm) and ${}^5\text{D}_0 \rightarrow {}^7\text{F}_2$ (615) and ${}^5\text{D}_0 \rightarrow {}^7\text{F}_3$ (628 nm) transitions, which are the typical emission properties of the Eu^{3+} activator.

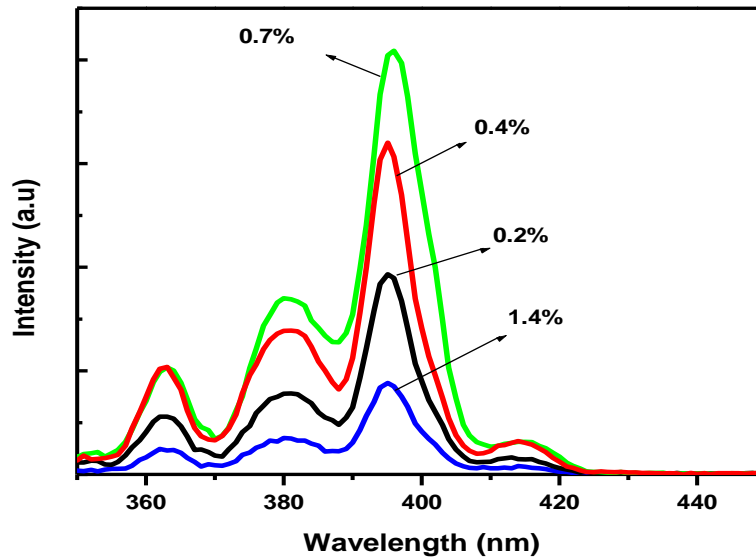


Figure 6.5: Excitation spectra of $Y_3Al_5O_{12}:Eu^{3+}$ phosphor with different concentration of Eu^{3+}

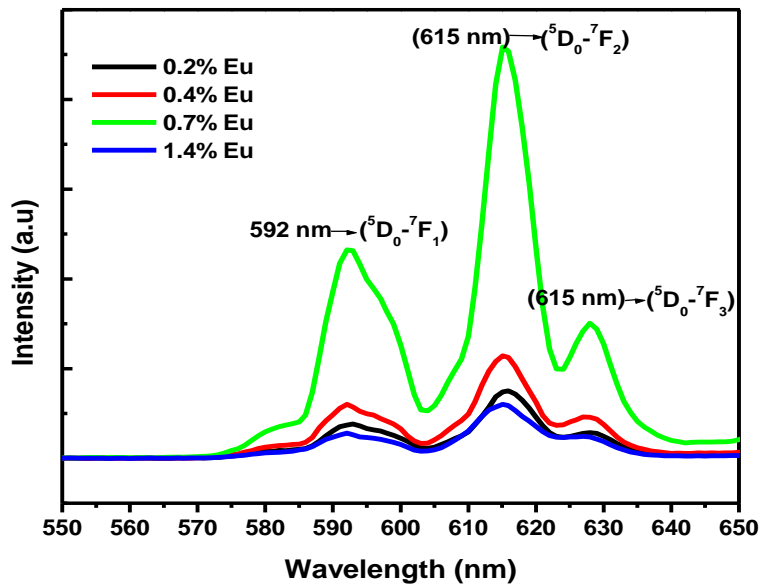


Figure 6.6: Emission spectra of $Y_3Al_5O_{12}:Eu^{3+}$ phosphor with different Eu^{3+} concentration

It can be seen in Figure 6.7 that emission intensity increased significantly with the concentration of europium, because the transition energy from $Y_3Al_5O_{12}$ to Eu^{3+} was increased by the concentration quenching effect resulting from the added Eu^{3+} . When the concentration increased from 0.4 mol% to 0.7 mol% the emission intensity significantly increased. At Eu concentration of 1.4 mol%, emission intensity became lower than that at 0.7 mol%. At a high concentration of Eu^{3+} the non-radiative transition would lead to a decrease in emission intensity because the transition energy between two activators Eu^{3+} and Eu^{3+} increased by dipole-dipole interaction [14].

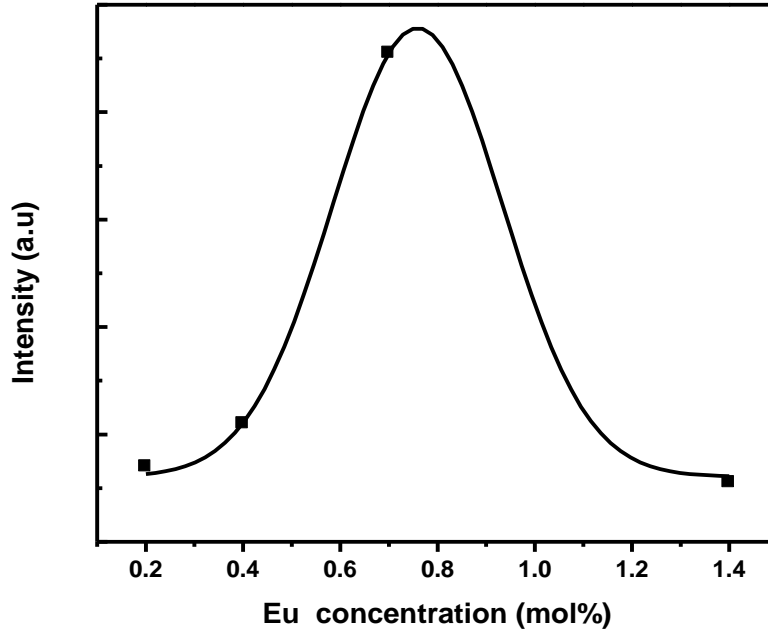


Figure 6.7: PL maximum intensity as a function of Eu^{3+} concentration

Figure 6.8 shows the decay curves of $\text{Y}_3\text{Al}_5\text{O}_{12}:\text{Eu}^{3+}$ phosphor with different concentration of Eu. The decay behavior can be expressed by

$$I = A_1 \exp(-t/\tau_1) + A_2 \exp(-t/\tau_2) \quad (6.1)$$

Where I represent the phosphorescent intensity: A_1 and A_2 are constants: t is time: τ_1 and τ_2 are the decay times for exponential components. The decay parameters of τ_1 and τ_2 are listed in table 5. Results indicate that the intensity of the phosphorescence decreased quickly at first and then at a slower rate. The curve of the sample doped with the high concentration of 1.4% displays a lower intensity. When the concentration increases from 0.2 to 0.7 the luminescent of the curve also increased. This means that at high concentration the brightness of the phosphor is poor.

Table 6: Decay parameters of the $Y_3Al_5O_{12}:Eu^{3+}$ phosphor with different Eu concentrations

Eu ³⁺ %	0.2%	0.4%	0.7%	1.4%
Component	Decay constants			
τ_1 (ms)	0.58	1.06	1.19	0.71
τ_2 (ms)	2.11	2.54	2.48	2.17

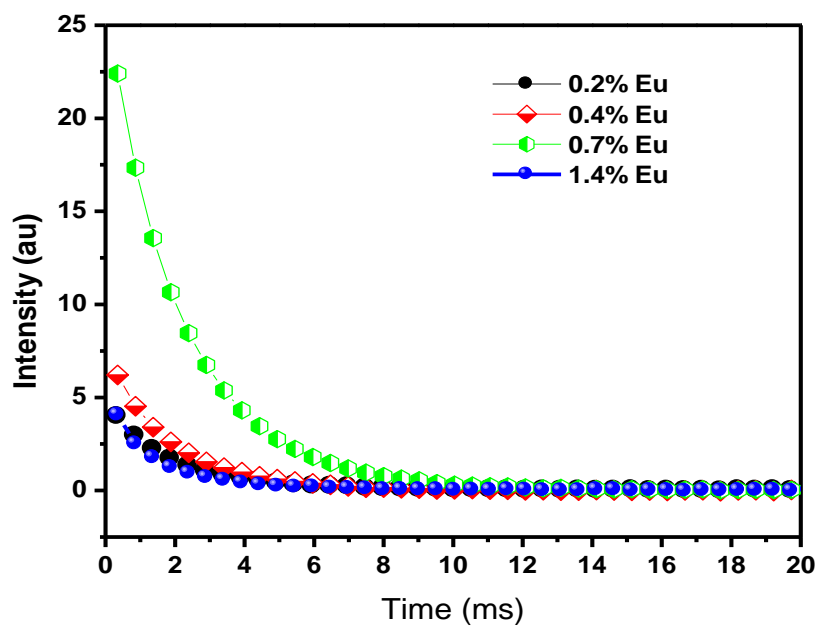


Figure 6.8: Decay curves of $Y_3Al_5O_{12}:Eu^{3+}$

6.4 Conclusion

Red emitting $Y_3Al_5O_{12}:Eu^{3+}$ phosphor was successfully synthesized with a solution combustion method. XRD spectra showed a tetragonal crystal structure of $Y_3Al_5O_{12}$. FTIR spectra showed all the chemical bonds found in $Y_3Al_5O_{12}:Eu^{3+}$ phosphor. The PL spectra showed emission peaks from 592 nm, 615 nm and 628 nm corresponding to $^5D_0 \rightarrow ^7F_1$, $^5D_0 \rightarrow ^7F_2$ and $^5D_0 \rightarrow ^7F_3$ respectively and the maximum emission wavelength was near 615 nm. The europium doping concentrations enhanced the luminescence up to 0.7% doping and quenches when concentration increased up to 1.4%. The decay spectra show a lower luminescence at higher concentrations.

References

- [1] W. Sea-Fue, K. R. Koteswara, W. Yu-Chuan, W. Yuh-Ruey, H. Yung-Fu, H. Chian-You, *Int. J. Appl. ceramic. Technol.*, **6** [4], 479-478. (2009)
- [2] L. Chung-Hsin, H. Wei-Tse, J. Dhanataj, R. Jagannathan, *J. of European Ceramic Society*, **24**, 3723-3729. (2004)
- [3] L. Zhang, H. Xia, Y. Qiu, D. Wang, H. Jiang, *J. of Rare earth*, **28**, p. 236. (2010)
- [4] Y. Ravishanker, F. K. Atif, Y. Ashish, C. Harish, H. Divi, K. Biping Kr., S. Virendra, C. Santa, *Optics Express*, **17**, 24. (2009)
- [5] Y. Min-Jae, I. Jung-Hyun, L. Hyeon-Cheol, L. Chang Ha, *J. Korean. Chem. Eng.*, **23**(5), 842-846. (2006)
- [6] L. Ji-Guang, I. Takayasu, L. Jong-Heun, M. Toshiyuki, *J. Mater. Res.* **15**, No. 11. (2000)
- [7] H. Yukiya, S. kazuei, U. Haruo, A. Tadafumi, T. Hirotsugu, A. Kunio, *J. of Mater. Chem.*, **9**, 2671-2674. (1999)
- [8] C. Shin-Hei, K. Nam-Hoon, Y. Young-Hoon, C. Sung-Churl, *J. of Ceramic Processing Research*, **7**, 62-65. (2006)
- [9] S. Huajie, C. Donghua, *Luminescence*, **22**, 554-558. (2007)
- [10] B. S. Barros, P. S. Melo, R. H. G. A. Kiminami, A. C. F. M. Costa, G. F. de Sá, alves Jr S, *J. MasteSci*, **41**, 4744-4748 (2006)
- [11] Y. Xibin, Z. Chunlei, H. Xianghong, P. Zifei, Y. Shi-ping, *Materials Letters*, **58**, 1087-1091. (2004)
- [12] V. Singh, S. Watanabe, T. K. GunduRao, *J. Fluoresce*, **21**, 313-320. (2011)
- [13] G. Xia, S. Zhou, J. Zhang, S. Wang, Y. Liu, J. Xu, *J. of Crystal Growth*, **283**, 257-262. (2005)
- [14] J. H. In, H. C. Lee, M. J. Yoon, K. K. Lee, J. W. Lee, C. H. Lee, *J. of Supercritical Fluids*, **40**, 389-396. (2007)

Chapter VII

General conclusion and summary

7.1 Thesis summary

In this study the $\text{SrAl}_2\text{O}_4:\text{Ce}^{3+}$, $\text{SrAl}_2\text{O}_4:\text{Tb}^{3+}$, $\text{CaAl}_x\text{O}_y:\text{Tb}^{3+}$, $\text{Y}_3\text{Al}_5\text{O}_{12}:\text{Eu}^{3+}$ phosphors were successfully synthesized by the solution combustion method using urea as a fuel. The solution combustion method is a low temperature (500 °C), fast (short preparation times ~few minutes) and efficient synthesis method involving an exothermic reaction that liberates enormous volumes of gases.

The $\text{SrAl}_2\text{O}_4:\text{Ce}^{3+}$, $\text{SrAl}_2\text{O}_4:\text{Tb}^{3+}$, $\text{CaAl}_x\text{O}_y:\text{Tb}^{3+}$, $\text{Y}_3\text{Al}_5\text{O}_{12}:\text{Eu}^{3+}$ powder phosphors were characterized. The characterization of these phosphors was carried out using different techniques. SEM coupled with an energy dispersive X-ray spectrometer (EDS) was used to determine the morphology and elemental composition of the phosphors. Luminescent and structural properties of the phosphors were analyzed by photoluminescence spectrophotometer. Chemical bonds of the matrix were also investigated using FTIR. The crystallite structure of the phosphors together with the particle sizes were determined by using the X-ray diffractometer.

The $\text{SrAl}_2\text{O}_4:\text{Ce}^{3+}$ with different concentration of cerium was successfully characterized. The diffraction peaks associate with monoclinic structure was obtained. The average particle sizes of the phosphor were estimated using the Scherrer's equation, and was found to be 47 nm. The broad emission band consisting of two peaks at 374 nm and 384 nm were obtained with concentration quenching observed for higher dopant concentration. SEM image exhibit the agglomerated particles and at high magnification it shows the nanorods-like particles. EDS confirmed the presence of the elements in the $\text{SrAl}_2\text{O}_4:\text{Ce}^{3+}$.

The particle sizes of main peaks of the phosphor $\text{SrAl}_2\text{O}_4:\text{xTb}^{3+}$ were obtained from the XRD. The major peaks in the patterns correspond to a monoclinic structure according to the JCPDS file (74-0794) standard data and some unknown peaks were observed. A broad band centered on 229nm was observed on emission spectra. $\text{SrAl}_2\text{O}_4:\text{xTb}^{3+}$ phosphor emits in the green between 489—622 nm which agrees with the emission characteristics of Tb^{3+} . The maximum emission intensity was obtained for 0.25 mol% Tb^{3+} ; however intensity decreases with increasing concentrations are attributed to concentration quenching. Morphology of the powders reflected the inherent of the combustion process by forming the pores and the voids. The decay curves show a low intensity at high concentration of 2 mol% Tb^{3+} .

$\text{CaAl}_x\text{O}_y:\text{xTb}^{3+}$ doped with different concentration of Tb^{3+} was successfully synthesized by solution combustion method. The monoclinic structure of CaAl_2O_4 and was obtained. The luminescence properties were investigated. The optimum PL intensity was observed at $x=2\text{mol}\%$. The emission bands can be attributed to the transition of $^5\text{D}_4$ state to the $^7\text{F}_J$ ($J = 6, 5, 4, 3$). Long afterglow decay curves were observed, the luminescence brightness was improved by increasing the Tb^{3+} concentration thus prolonging the long afterglow time. All the elements found in $\text{CaAl}_x\text{O}_y:\text{xTb}^{3+}$ was obtained by the use of energy dispersive spectroscopy.

The $\text{Y}_3\text{Al}_5\text{O}_{12}:\text{Eu}^{3+}$ ($\text{Eu}^{3+}=0.2, 0.4, 0.7, \text{ and } 1.4 \text{ mol}\%$) phosphor were successfully synthesize and characterized. the PL emission peaks from Eu^{3+} ions at 592, 615, and 628 nm are due to the $^5\text{D}_0 \rightarrow ^7\text{F}_1$ and $^5\text{D}_0 \rightarrow ^7\text{F}_2$ and $^5\text{D}_0 \rightarrow ^7\text{F}_3$ transitions, respectively were observed. emission spectrum were observed in the red spectral area. maximum PL intensity was shown by a sample with 0.7 mol % doping concentration of Eu^{3+} . formation of agglomerated particles were observed. All the chemical bonds were observed in Fourier transform infrared. The x-ray peaks were match with standard peaks of $\text{Y}_3\text{Al}_5\text{O}_{12}$ phase (JCPDS 09-0310), however the impurities were observed.

7.2 Future work

The XRD structure of the phosphors showed the impurities, the improvement of the synthesis should be made. The PL emission spectra of $\text{CaAl}_x\text{O}_y:\text{Tb}^{3+}$ showed the optimum intensity at $x=2$ mol%, therefore the terbium concentration should be increased further to see if the intensity will increase or quench. In this study the single dopant phosphors were synthesized, therefore it is important to improve the long afterglow of the phosphors by codoping.

Conference attended

K.E Foka, F.B Dejene and HC Swart, Synthesis and characterization of a green $\text{CaAl}_x\text{O}_y:\text{Tb}^{3+}$ phosphor using solution combustion method.

56th Annual Conference of the South African Institute of Physics (SAIP), hosted by UNISA, St Georges Hotel and Convention Centre, Pretoria, 12 – 15 July 2011